Mon. Not. R. Astron. Soc. **295,** 319–336 (1998)

The formation of galactic discs

H. J. Mo,* Shude Mao* and Simon D. M. White*

Max-Planck-Institut für Astrophysik, Karl-Schwarzschild-Strasse 1, 85748 Garching, Germany

Accepted 1997 September 29. Received 1997 September 26; in original form 1997 July 16

ABSTRACT

We study the population of galactic discs expected in current hierarchical clustering models for structure formation. A rotationally supported disc with exponential surface density profile is assumed to form with a mass and angular momentum which are fixed fractions of those of its surrounding dark halo. We assume that haloes respond adiabatically to disc formation, and that only stable discs can correspond to real systems. With these assumptions the predicted population can match both present-day discs and the damped Lyα absorbers in QSO spectra. Good agreement is found provided that: (i) the masses of discs are a few per cent of those of their haloes; (ii) the specific angular momenta of discs are similar to those of their haloes; (iii) present-day discs were assembled recently (at $z \le 1$). In particular, the observed scatter in the size–rotation velocity plane is reproduced, as are the slope and scatter of the Tully–Fisher (TF) relation. The zero-point of the TF relation is matched for a stellar mass-to-light ratio of 1 to 2 h in the I-band, consistent with observational values derived from disc dynamics. High-redshift discs are predicted to be small and dense, and could plausibly merge together to form the observed population of elliptical galaxies. In many (but not all) currently popular cosmogonies, discs with rotation velocities exceeding 200 km s^{-1} can account for a third or more of the observed damped Lyα systems at $z \sim 2.5$. Half of the lines of sight to such systems are predicted to intersect the absorber at $r \gtrsim 3\,h^{-1}$ kpc and about 10 per cent at $r > 10\,h^{-1}$ kpc. The cross-section for absorption is strongly weighted towards discs with large angular momentum and therefore large size for their mass. The galaxy population associated with damped absorbers should thus be biased towards low surface brightness systems.

Key words: galaxies: formation – galaxies: spiral – galaxies: structure – cosmology: theory – dark matter.

1 INTRODUCTION

An important goal of cosmology is to understand how galaxies form. In standard hierarchical models dissipationless dark matter aggregates into larger and larger clumps as gravitational instability amplifies the weak density perturbations produced at early times. Gas associated with such dark haloes cools and condenses within them, eventually forming the galaxies we see today. These two aspects of galaxy formation are currently understood at very different levels. Gravitational processes that determine the abundance, the internal structure and kinematics, and the formation paths of the dark haloes can be simulated in great detail using N-body methods. Well-tested analytic models are now available for describing these properties of the halo population. The growth of the dark haloes is not much affected by the baryonic components, but determines how they are assembled into non-linear units. Gas cools and collects at the centre of each dark halo until it produces an independent self-gravitating unit which can form stars, heating and enriching the rest of the gas, and perhaps even ejecting it from the halo. These star formation and feedback processes are not understood in detail and can be modelled or simulated only crudely. Furthermore, as haloes merge to form groups and clusters of galaxies, the cluster members interact and merge both with each other and with the intracluster gas. It will not soon be possible to simulate galaxy formation *ab initio*. At least the star formation and feedback processes must be put in ad hoc based on observations of real galaxies.

In a first exploration of the galaxy population expected in this hierarchical picture, White & Rees (1978) calculated the expected luminosity function. The observed characteristic luminosity of galaxies could be reproduced provided (i) that feedback prevents efficient conversion of gas into stars in early objects, and (ii) that merging of galaxies is inefficient as groups and clusters of galaxies

*E-mail: hom@mpa-garching.mpg.de (HJM); smao@mpa-garching.mpg.de (SM); swhite@mpa-garching.mpg.de (SDMW)

build up. The models appeared to overproduce faint galaxies. The formation of galaxy discs within this scheme was studied by Fall & Efstathiou (1980). They showed that if galactic spin is produced by tidal torques acting at early times, then extended massive haloes are necessary if discs as large as those observed are to form by the present day. They also found that plausible initial angular momentum distributions for the gas could lead to near-exponential density profiles for the final disc. More recent analytic work has refined the calculation of global properties of galaxies: for example, the distributions of luminosity, colour, morphology and metallicity can all be calculated explicitly in currently popular cosmogonies (e.g. White & Frenk 1991; Kauffmann, White & Guiderdoni 1993; Cole et al. 1994; Baugh et al. 1997). There has, however, been relatively little work on the internal structure of galaxies. Kauffmann (1996b) studied the accumulation, star formation and chemical enrichment histories of individual discs, linking them to damped Lyα absorbers at high redshift, but she did not consider the scatter in angular momentum for discs of a given mass and the resulting scatter in their present-day properties. Dalcanton, Spergel & Summers (1997, hereafter DSS) considered the latter issue in some detail, but did not tie their model explicitly to its cosmogonical context or consider its implications for disc evolution. There have also been surprisingly few well-resolved simulations of galaxy formation from initial conditions that properly reflect the hierarchical model. So far all have failed to produce viable models for observed spirals because excessive transfer of angular momentum from gas to dark matter results in overly small discs (e.g. Navarro & Steinmetz 1997).

In the present paper, we again address the problem of disc formation in hierarchical cosmogonies, formulating a simple model based on four key assumptions: (1) the mass of a disc is some fixed fraction of that of the halo in which it is embedded; (2) the angular momentum of the disc is also a fixed fraction of that of its halo; (3) the disc is a thin centrifugally supported structure with an exponential surface density profile; and (4) only dynamically stable systems can correspond to real galaxy discs. We derive the abundance of haloes in any specific cosmogony from the Press–Schechter formalism, we model their density profiles using the precepts of Navarro, Frenk & White (1996, 1997, hereafter NFW), and we assume their angular momentum distribution to have the near-universal form found in *N*-body simulations. (See Lacey & Cole 1994 for a summary of how well these analytic models fit simulation results.) Our four assumptions are then sufficient to predict the properties of the disc population, once values are assumed for the mass and angular momentum fractions and the redshift of disc formation. A mass-to-light ratio for the disc stars must also be assumed in order to compare with the luminosities of observed discs. Our assumptions are similar to those of DSS but differ in detail. We calculate many of the same properties they do, but in addition we address broader issues such as the evolution of discs, the dependence of the disc population on cosmological parameters, and the link with QSO absorption lines.

The outline of our paper is as follows. Section 2 presents our modelling assumptions in detail. To clarify the scaling of disc properties with model parameters, we first treat haloes as singular isothermal spheres and neglect the gravitational effects of the discs. We then consider the more realistic NFW profiles and include the gravitational effects of the discs. In Sections 3 to 5, we describe the predicted properties of present-day discs, we discuss TF relations, we compare high-redshift discs with QSO absorption line systems, and we study the effect of a non-rotating central bulge. Finally, in Section 6, we discuss other issues related to our model.

2 MODELS FOR DISCS IN HIERARCHICAL COSMOGONIES

2.1 The cosmogonies

In cold dark matter (CDM) cosmogonies the evolution of the dark matter is determined by the parameters of the background cosmological model and by the power spectrum of the initial density fluctuations. The relevant cosmological parameters are the Hubble constant $H_0 = 100h\,\mathrm{km\,s^{-1}\,Mpc^{-1}}$, the total matter density Ω_0, the mean density of baryons $\Omega_{\mathrm{B},0}$, and the cosmological constant $\Omega_{\Lambda,0}$. The last three are all expressed in units of the critical density for closure. The power spectrum $P(k)$ is specified in CDM models by an amplitude, conventionally quoted as σ_8, the rms linear overdensity at $z = 0$ in spheres of radius $8\,h^{-1}$ Mpc, and by a characteristic scale $\Gamma = \Omega_0 h/R$, where R is the current radiation density in units of the standard value corresponding to a $T = 2.73$ K blackbody photon field and equilibrium abundances of three massless neutrinos. For such cosmogonies the abundance of haloes as a function of mass and redshift can be calculated quite accurately using the Press–Schechter formalism, while their radial density profiles can be calculated as a function of these same variables using the results of Navarro et al. (1997). We give some details of how we implement these formalisms in the Appendix.

In the main body of this paper we will compare results for four different CDM cosmogonies. These are specified by particular values of the parameter set $(\Omega_0, \Omega_{\Lambda,0}, h, \Gamma, \sigma_8)$. We do not explicitly need to assume a value for the baryon density $\Omega_{\mathrm{B},0}$, although for consistency we should require $\Omega_{\mathrm{B},0} > m_{\mathrm{d}}\Omega_0$ where m_{d} is the ratio of disc mass to halo mass adopted (and assumed universal) in our models. This ensures that the disc mass is less than the total initial baryon content of the halo. Our four cosmogonies are:

(i) the standard cold dark matter model (SCDM), with $\Omega_0 = 1$, $\Omega_{\Lambda,0} = 0$, $h = 0.5$ $\Gamma = 0.5$ and $\sigma_8 = 0.6$;
(ii) a *COBE*-normalized cold dark matter model (CCDM), which has the same parameters as SCDM, except that $\sigma_8 = 1.2$;
(iii) a τCDM model, with $\Omega_0 = 1$, $\Omega_{\Lambda,0} = 0$, $h = 0.5$, $\Gamma = 0.2$ and $\sigma_8 = 0.6$; and
(iv) a ΛCDM model, with $\Omega_0 = 0.3$, $\Omega_{\Lambda,0} = 0.7$, $h = 0.7$, $\Gamma = 0.2$ and $\sigma_8 = 1.0$.

The τCDM model could be realised if the τ-neutrino were unstable to decay into other neutrinos and had a mass and lifetime satisfying $m_\tau t_\tau \approx 17$keV yr (Efstathiou, Bond & White 1992). On the relevant scales the power spectrum in this model is quite similar to that of a mixed dark matter (MDM) model with 20 per cent of the critical density in stable neutrinos. The values of σ_8 adopted for τCDM and ΛCDM are consistent both with the observed abundance of rich clusters (e.g. White, Efstathiou & Frenk 1993; Mo, Jing & White 1996) and with observed anisotropies in the cosmic microwave background (e.g. White & Scott 1996), whereas the value for SCDM is consistent only with the cluster normalization and that for CCDM only with the *COBE* normalization.

2.2 Non-self-gravitating discs in isothermal spheres

Many of the properties we predict for galaxy discs can be understood using a very simple model in which dark haloes are treated as singular isothermal spheres and the gravitational effects of the discs themselves are neglected. We will examine the limitations of this rather crude treatment in Section 2.3.

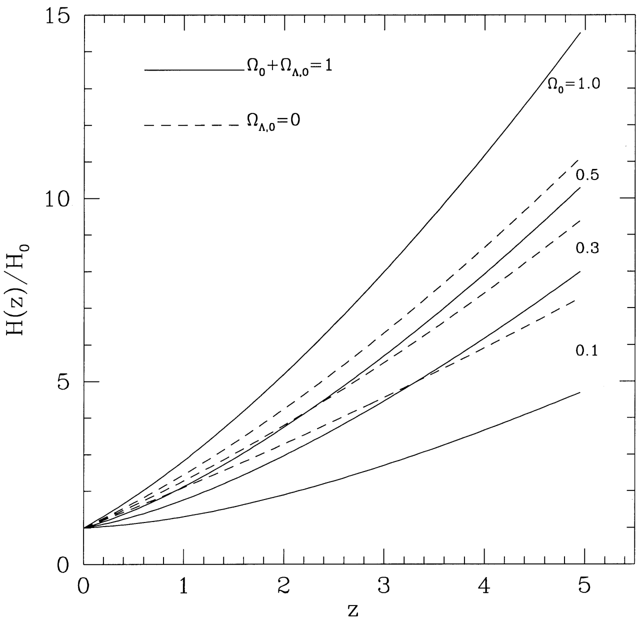

Figure 1. The Hubble constant (in units of its present value) as a function of redshift for flat ($\Omega_0 + \Omega_{\Lambda,0} = 1$) and open models with various Ω_0.

For a singular isothermal sphere the density profile is just

$$\rho(r) = \frac{V_c^2}{4\pi G r^2}, \tag{1}$$

where the circular velocity V_c is independent of radius. Based on the spherical collapse model (Gunn & Gott 1972; Bertschinger 1985; Cole & Lacey 1996), we define the limiting radius of a dark halo to be the radius r_{200} within which the mean mass density is $200\rho_{\rm crit}$, where $\rho_{\rm crit}$ is the critical density for closure at the redshift z when the halo is identified. Thus, the radius and mass of a halo of circular velocity V_c seen at redshift z are

$$r_{200} = \frac{V_c}{10H(z)}; \quad M = \frac{V_c^2 r_{200}}{G} = \frac{V_c^3}{10GH(z)}, \tag{2}$$

where

$$H(z) = H_0\left[\Omega_{\Lambda,0} + (1-\Omega_{\Lambda,0}-\Omega_0)(1+z)^2 + \Omega_0(1+z)^3\right]^{1/2} \tag{3}$$

is the Hubble constant at redshift z. The redshift dependence of halo properties, and so of the discs which form within them, is determined by $H(z)$. In order to understand this dependence better, Fig. 1 shows $H(z)/H_0$ as a function of z for open and flat cosmologies with various Ω_0. $H(z)$ increases more rapidly with z in universes with larger Ω_0. For a given Ω_0, the increase is more rapid for an open universe than for a flat universe. At $z \gtrsim 1$, the ratio $H(z)/H_0$ is about twice as large in an Einstein–de Sitter universe as in a flat universe with $\Omega_0 = 0.3$. As a result of this difference, the properties of high-redshift discs will depend significantly on Ω_0 and $\Omega_{\Lambda,0}$.

We assume that the mass which settles into the disc is a fixed fraction m_d of the halo mass. The disc mass is then

$$M_d = \frac{m_d V_c^3}{10GH(z)} \approx 1.7\times10^{11} h^{-1}\,{\rm M}_\odot \left(\frac{m_d}{0.05}\right)\left(\frac{V_c}{250\,{\rm km\,s^{-1}}}\right)^3 \left[\frac{H(z)}{H_0}\right]^{-1}. \tag{4}$$

Except in Section 5 where we investigate the effects of including a central bulge, we distinguish only halo and disc components, and we assume the discs to be thin, to be in centrifugal balance, and to have exponential surface density profiles,

$$\Sigma(R) = \Sigma_0 \exp(-R/R_d). \tag{5}$$

Here R_d and Σ_0 are the disc scalelength and central surface density, and are related to the disc mass through

$$M_d = 2\pi\Sigma_0 R_d^2. \tag{6}$$

If the gravitational effect of the disc is neglected, its rotation curve is flat at the level V_c and its angular momentum is just

$$J_d = 2\pi\int V_c\Sigma(R)R^2{\rm d}R = 4\pi\Sigma_0 V_c R_d^3 = 2M_d R_d V_c. \tag{7}$$

We assume this angular momentum to be a fraction j_d of that of the halo, i.e.

$$J_d = j_d J, \tag{8}$$

and we relate J to the spin parameter λ of the halo through the definition

$$\lambda = J|E|^{1/2}G^{-1}M^{-5/2}, \tag{9}$$

where E is the total energy of the halo. Equations (7) and (8) then imply that

$$R_d = \frac{\lambda G M^{3/2}}{2V_c|E|^{1/2}}\left(\frac{j_d}{m_d}\right). \tag{10}$$

The total energy of a truncated singular isothermal sphere is easily obtained from the virial theorem by assuming all particles to be on circular orbits:

$$E = -\frac{GM^2}{2r_{200}} = -\frac{MV_c^2}{2}. \tag{11}$$

On inserting this into equation (10) and using equations (2) and (6) we get

$$R_d = \frac{1}{\sqrt{2}}\left(\frac{j_d}{m_d}\right)\lambda r_{200}$$
$$\approx 8.8h^{-1}\,{\rm kpc}\left(\frac{\lambda}{0.05}\right)\left(\frac{V_c}{250\,{\rm km\,s^{-1}}}\right)\left[\frac{H}{H_0}\right]^{-1}\left(\frac{j_d}{m_d}\right), \tag{12}$$

and

$$\Sigma_0 \approx 4.8\times10^{22}h\,{\rm cm^{-2}}m_{\rm H}\left(\frac{m_d}{0.05}\right)\left(\frac{\lambda}{0.05}\right)^{-2}$$
$$\times\left(\frac{V_c}{250\,{\rm km\,s^{-1}}}\right)\left[\frac{H(z)}{H_0}\right]\left(\frac{m_d}{j_d}\right)^2, \tag{13}$$

where $m_{\rm H}$ is the mass of a hydrogen atom. Using equations (5), (12) and (13), we can also obtain the limiting radius, R_l, at which the disc surface density drops below some critical hydrogen column N_l (which must be less than $\Sigma_0/m_{\rm H}$):

$$R_l \approx R_d\left\{5.5 + \ln\left[\left(\frac{m_d}{0.05}\right)\left(\frac{m_d}{j_d}\right)^2\left(\frac{\lambda}{0.05}\right)^{-2}\right.\right.$$
$$\left.\left.\times\left(\frac{V_c}{250\,{\rm km\,s^{-1}}}\right)\frac{H(z)}{H_0}\left(\frac{N_l}{2\times10^{20}h\,{\rm cm^{-2}}}\right)^{-1}\right]\right\}. \tag{14}$$

This radius depends on r_{200}, λ and j_d/m_d primarily through the scalelength, R_d.

Equations (4) and (12)–(14) give the scalings of disc properties with respect to a variety of physical parameters. These properties are completely determined by the values of V_c, m_d, j_d, λ and $H(z)$; other cosmological parameters, such as z, Ω_0 and $\Omega_{\Lambda,0}$, affect discs only indirectly through $H(z)$. Since $H(z)$ increases with z, discs of given circular velocity are less massive, are smaller and have higher surface densities at higher redshifts. At a given redshift, they are larger and less compact in haloes with larger λ, because they contract less before coming to centrifugal equilibrium. We will approximate the distribution of λ by

$$p(\lambda)\,\mathrm{d}\lambda = \frac{1}{\sqrt{2\pi}\sigma_\lambda}\exp\left[-\frac{\ln^2(\lambda/\bar{\lambda})}{2\sigma_\lambda^2}\right]\frac{\mathrm{d}\lambda}{\lambda}, \tag{15}$$

where $\bar{\lambda} = 0.05$ and $\sigma_\lambda = 0.5$. This function is a good fit to the N-body results of Warren et al. (1992; see also Cole & Lacey 1996; Steinmetz & Bartelmann 1995; Catelan & Theuns 1996) except possibly at very small λ; note that the function is narrower than the distribution used by DSS. Since the dependence of $p(\lambda)$ on M and $P(k)$ is weak, we will not consider it further. This model for $p(\lambda)$ is plotted as the dotted curve in Fig. 10 (see below). The distribution peaks around $\lambda = 0.04$, and has a width of about 0.05. Its 10, 50 and 90 per cent points are near $\lambda = 0.025$, 0.05 and 0.1, respectively. Thus we see from equations (12) and (13) that about 10 per cent of discs of given circular velocity will be more than twice the size of the typical disc, and so have less than a quarter of the typical surface density, while about 10 per cent will be less than half the typical size, and so have more than four times the typical surface density. (The latter 10 per cent may be unstable – see Section 3.2.)

Disc masses are, of course, directly proportional to m_d, the fraction of the halo mass we assume them to contain. For simplicity we will assume this fraction to be the same for all discs, but even in this case it is unclear what value of m_d is appropriate. A plausible upper limit is the baryon fraction of the Universe as a whole, $f_\mathrm{B} \equiv \Omega_{\mathrm{B},0}/\Omega_0$, but the efficiency of forming discs could be quite low, implying that m_d could be substantially smaller than f_B. Taking a big bang nucleosynthesis value for the baryon density, $\Omega_{\mathrm{B},0} = 0.015h^{-2}$ (e.g. Walker et al. 1991, but see Turner 1996), gives an upper limit on m_d in the range 0.05 to 0.1 for the cosmological models we consider (see Section 2.1).

If the specific angular momentum of the material which forms the disc is the same as that of the halo, then $j_\mathrm{d}/m_\mathrm{d} = 1$. This has been the standard assumption in modelling disc formation since the work of Fall & Efstathiou (1980), but it is unclear if it is appropriate, particularly if the efficiency of disc formation, $m_\mathrm{d}/f_\mathrm{B}$, is significantly less than unity. Even when this efficiency is high, numerical simulations of spiral galaxy formation have tended to find $j_\mathrm{d}/m_\mathrm{d}$ values well below unity (e.g. Navarro & White 1994; Navarro & Steinmetz 1997). Equation (12) shows that disc sizes are directly proportional to $j_\mathrm{d}/m_\mathrm{d}$, and we will find below that values close to unity are required to fit observed spirals. This agrees with the fact that the simulations did indeed produce galaxies with too little angular momentum. Most of our discussion will assume $j_\mathrm{d} = m_\mathrm{d}$, but we will comment on the effects of changing m_d and j_d independently.

The disc of our own Galaxy has a mass of about $6\times10^{10}\,\mathrm{M}_\odot$. Its scalelength and circular velocity (measured at the solar radius, $\mathrm{R}_\odot \sim 8\,\mathrm{kpc}$) are $R_\mathrm{d} \sim 3.5\,\mathrm{kpc}$ and $V_\mathrm{c} \sim 220\,\mathrm{km\,s^{-1}}$ (see Binney & Tremaine 1987, p. 17). Since the Milky Way appears to be a typical Sbc galaxy, it is interesting to see whether a disc with these parameters is easily accommodated. Equation (4) together with Fig. 1 implies that Milky Way-like discs cannot form at $z > 1$ in a universe with $\Omega_0 \sim 1$; for our nucleosynthesis value of f_B the disc mass for $V_\mathrm{c} = 220\,\mathrm{km\,s^{-1}}$ is too small even if discs are assumed to form with maximal efficiency. The constraints are weaker for a low-Ω_0 universe, because f_B is larger and $H(z)$ increases less rapidly with z. A similar conclusion can be derived from R_d. At high redshift the disc scalelength for $V_\mathrm{c} = 220\,\mathrm{km\,s^{-1}}$ is too small to match the observed value unless $\lambda \gg 0.05$. Such high values of λ are associated with only a small fraction of haloes, and so late formation is required for the bulk of the disc population. As we will see later, these constraints become stronger in more realistic models.

If we assume that all discs have the same stellar mass-to-light ratio, $\Upsilon_\mathrm{d} \equiv M_\mathrm{d}/L_\mathrm{d}$ (in solar units), we can cast equation (4) into a form similar to the TF relation:

$$L_\mathrm{d} = A\left(\frac{V_\mathrm{c}}{250\,\mathrm{km\,s^{-1}}}\right)^\alpha, \tag{16}$$

where $\alpha = 3$ is the slope, and

$$A = 1.7\times10^{11}h^{-1}\mathrm{L}_\odot\Upsilon_\mathrm{d}^{-1}\left(\frac{m_\mathrm{d}}{0.05}\right)\left[\frac{H(z)}{H_0}\right]^{-1} \tag{17}$$

is the 'zero-point'. Notice that λ does not appear in these equations. As a result, all the discs assembled at a given time are predicted to lie on a scatter-free TF relation despite the fact that there is substantial scatter in their scale radii and surface densities. The zero-point of this TF relation can, however, depend on the redshift of assembly, being lower at higher redshifts if the product $\Upsilon(z)H(z)$ is larger. For I-band luminosities the observed value of α is very close to 3 (Willick et al. 1995, 1996; Giovanelli et al. 1997). Since stellar population synthesis models suggest that Υ_d should vary only slightly in this band, we can take this as confirmation of the approximate validity of our assumption that m_d is independent of V_c. The zero-point of the observed TF relation corresponds to a value of A of about $5\times10^{10}\,h^{-2}\,\mathrm{L}_\odot$ (Giovanelli et al. 1997). Since the expected value of the disc mass-to-light ratio is $\Upsilon_\mathrm{d} \approx 1.7h$ (see Section 3.4, below, and Bottema 1997), comparison with equation (17) again suggests that late assembly epochs are required; for the appropriate values of m_d the predicted zero-point would be too low if discs formed at high redshift.

The limiting radius R_l which we defined in equation (14) is chosen to be relevant to the damped Lyα absorption lines seen in QSO spectra. Such systems have H I column densities of $N_\mathrm{H\,I} \gtrsim 2\times10^{20}\,\mathrm{cm^{-2}}$, comparable to those of present-day galactic discs (see Wolfe 1995 for a review). For given V_c and λ, discs are smaller at higher redshifts. As a result the cross-section for damped Lyα absorption decreases with z. As one can see from equation (14), the limiting radius for damped absorption is roughly $\mathrm{R}_\mathrm{l} = 5.5R_\mathrm{d}$. For $V_\mathrm{c} \sim 200\,\mathrm{km\,s^{-1}}$ and $\lambda \sim 0.05$, we find R_l between 5 and $10\,h^{-1}\,\mathrm{kpc}$ at $z \sim 3$ for Ω_0 between 1 and 0.3. Given the distribution of dark haloes as a function of λ and V_c, it is clearly possible to calculate not only the total cross-section for damped absorption along a random line of sight, but also the distributions of λ, V_c, $N_\mathrm{H\,I}$ and the impact parameter (i.e. the distance between the centre of the absorbing disc and the line of sight to the QSO) for the systems actually seen as damped absorbers. We discuss this in detail in Section 4.

The model presented in this subsection is limited both because the dark haloes formed by dissipationless hierarchical clustering are only very roughly approximated by singular isothermal spheres, and because the gravitational effects of the discs are often not negligible. Despite this, most of the characteristic properties of this model are retained with only rather minor modifications in the more realistic model which we discuss next.

2.3 Self-gravitating discs in haloes with realistic profiles

In a recent series of papers Navarro, Frenk & White (1995, 1996, NFW) used high-resolution numerical simulations to show that the equilibrium density profiles of dark matter haloes of all masses in all dissipationless hierarchical clustering cosmogonies can be well-fitted by the simple formula

$$\rho(r) = \rho_{\rm crit} \frac{\delta_0}{(r/r_{\rm s})(1+r/r_{\rm s})^2}, \tag{18}$$

where $r_{\rm s}$ is a scale radius, and δ_0 is a characteristic overdensity. The logarithmic slope of this profile changes gradually from -1 near the centre to -3 at large radii. As before (and following NFW) we define the limiting radius of a virialized halo, r_{200}, to be the radius within which the mean mass density is $200\rho_{\rm crit}$. The mass within some smaller radius r is then

$$M(r) = 4\pi\rho_{\rm crit}\delta_0 r_{\rm s}^3 \left[\frac{1}{1+cx} - 1 + \ln(1+cx)\right], \tag{19}$$

where $x \equiv r/r_{200}$, and

$$c \equiv \frac{r_{200}}{r_{\rm s}} \tag{20}$$

is the halo concentration factor. The total mass of the halo is given by equation (19) with $x = 1$. Using equations (18)–(20), we can obtain a relation between the characteristic overdensity and the halo concentration factor,

$$\delta_0 = \frac{200}{3}\frac{c^3}{\ln(1+c) - c/(1+c)}. \tag{21}$$

We can obtain the total energy of the truncated halo as before by assuming all particles to be on circular orbits, calculating their total kinetic energy, and then using the virial theorem. This yields

$$\begin{aligned} E &= -G\frac{(4\pi\rho_{\rm crit}\delta_0 r_{\rm s}^3)^2}{2r_{\rm s}}\left[\frac{1}{2} - \frac{1}{2(1+c)^2} - \frac{\ln(1+c)}{1+c}\right] \\ &= -\frac{GM^2}{2r_{200}} f_{\rm c}, \end{aligned} \tag{22}$$

where

$$\begin{aligned} f_{\rm c} &= \frac{c}{2}\frac{1 - 1/(1+c)^2 - 2\ln(1+c)/(1+c)}{[c/(1+c) - \ln(1+c)]^2} \\ &\approx \frac{2}{3} + \left(\frac{c}{21.5}\right)^{0.7}. \end{aligned} \tag{23}$$

The approximation for $f_{\rm c}$ given above is accurate to within 1 per cent for the relevant range $5 < c < 30$ (to about 3 per cent for $0 < c < 50$). Comparing equation (22) with equation (11), we see that the total energy for an NFW profile differs from that for an isothermal sphere by the factor, $f_{\rm c}$, which depends only on the concentration factor.

If the gravitational effects of the disc were negligible, its rotation curve would simply follow the circular velocity curve of the unperturbed halo, $V_{\rm c}^2(r) = GM(r)/r$. This curve rises to a maximum at $r \approx 2r_{\rm s}$ and then falls gently at larger radii (see NFW). In fact, disc formation alters the rotation curve not only through the direct gravitational effects of the disc, but also through the contraction it induces in the inner regions of the dark halo. We analyse this effect by assuming that the halo responds adiabatically to the slow assembly of the disc, and that it remains spherical as it contracts; the angular momentum of individual dark matter particles is then conserved and a particle that is initially at mean radius, $r_{\rm i}$, ends up at mean radius, r, where

$$GM_{\rm f}(r)r = GM(r_{\rm i})r_{\rm i}. \tag{24}$$

In this formula $M(r_{\rm i})$ is given by the NFW profile (19) and $M_{\rm f}(r)$ is the total final mass within r. [See Barnes & White (1984) for a test of this adiabatic model; see also Blumenthal et al. (1986) for a related discussion.] The final mass is the sum of the dark matter mass inside the initial radius $r_{\rm i}$ and the mass contributed by the exponential disc. Hence

$$M_{\rm f}(r) = M_{\rm d}(r) + M(r_{\rm i})(1 - m_{\rm d}), \tag{25}$$

where, as before, $m_{\rm d}$, is the fraction of the total mass in the disc, and

$$M_{\rm d}(r) = M_{\rm d}\left[1 - \left(1 + \frac{r}{R_{\rm d}}\right){\rm e}^{-r/R_{\rm d}}\right]. \tag{26}$$

Here we implicitly assume that the baryons initially had the same density profile as the dark matter, and those that do not end up in the disc remain distributed in the same way as the dark matter. For a given rotation curve, $V_{\rm c}(R)$, the total angular momentum of the disc can be written as

$$\begin{aligned} J_{\rm d} &= \int_0^{r_{200}} V_{\rm c}(R) R\Sigma(R) 2\pi R {\rm d}R \\ &= M_{\rm d} R_{\rm d} V_{200} \int_0^{r_{200}/R_{\rm d}} {\rm e}^{-u} u^2 \frac{V_{\rm c}(R_{\rm d}u)}{V_{200}} {\rm d}u, \end{aligned} \tag{27}$$

where $V_{200} \equiv V_{\rm c}(r_{200})$ is unaffected by disc formation. In practice we can set the upper limit of integration to infinity because the disc surface density drops exponentially and $r_{200} \gg R_{\rm d}$. Substituting equation (22) into equation (9) and writing $J_{\rm d} = j_{\rm d}J$, we can use the argument of Section 2.2 to obtain

$$R_{\rm d} = \frac{1}{\sqrt{2}}\left(\frac{j_{\rm d}}{m_{\rm d}}\right)\lambda r_{200} f_{\rm c}^{-1/2} f_R(\lambda, c, m_{\rm d}, j_{\rm d}) \tag{28}$$

where

$$f_R(\lambda, c, m_{\rm d}, j_{\rm d}) = 2\left[\int_0^\infty {\rm e}^{-u} u^2 \frac{V_{\rm c}(R_{\rm d}u)}{V_{200}} {\rm d}u\right]^{-1}. \tag{29}$$

Comparing equation (28) with equation (12) we see two effects that cause the disc scalelength to differ from that in a singular isothermal sphere: the factor $f_{\rm c}^{-1/2}$ comes from the change in total energy resulting from the different density profile, while the factor $f_R(\lambda, c, m_{\rm d}, j_{\rm d})$ is due both to the different density profile and to the gravitational effects of the disc.

The rotation velocity $V_{\rm c}(r)$ is a sum in quadrature of contributions from the disc and from the dark matter:

$$V_{\rm c}^2(r) = V_{\rm c,d}^2(r) + V_{\rm c,DM}^2(r), \tag{30}$$

where

$$V_{\rm c,DM}^2(r) = G\big[M_{\rm f}(r) - M_{\rm d}(r)\big]/r, \tag{31}$$

and $V_{\rm c,d}(r)$ is the rotation curve that would be produced by the exponential disc alone. Note that when calculating the latter quantity the flattened geometry of the disc has to be taken into account (Binney & Tremaine 1987, p. 77). For a given set of parameters, V_{200}, c, λ, $m_{\rm d}$ and $j_{\rm d}$, equations (25), (26), (28) and (30) must be solved by iteration to yield the scalelength, $R_{\rm d}$, and the rotation curve, $V_{\rm c}(R)$. For example, we can start with a guess for $R_{\rm d}$ by setting $f_R = 1$ in equation (28). We can then obtain $M_{\rm d}(r)$ from equation (26). Substituting this into equation (25) and using equation (24), we can solve for $r_{\rm i}$ as a function of r and so obtain $M_{\rm f}(r)$ from equation (25). With this and with $V_{\rm c,d}^2(r)$ calculated for the assumed $R_{\rm d}$, we can get the disc rotation curve from equations (30) and (31). Inserting this into equation (29) and using equation (28) we then obtain a new value for $R_{\rm d}$. In practice this iteration converges rapidly, so that accurate values for both $R_{\rm d}$ and $V_{\rm c}(r)$ are easily obtained.

It is useful to have a fitting formula for f_R which allows this iterative procedure to be avoided. We find that the following

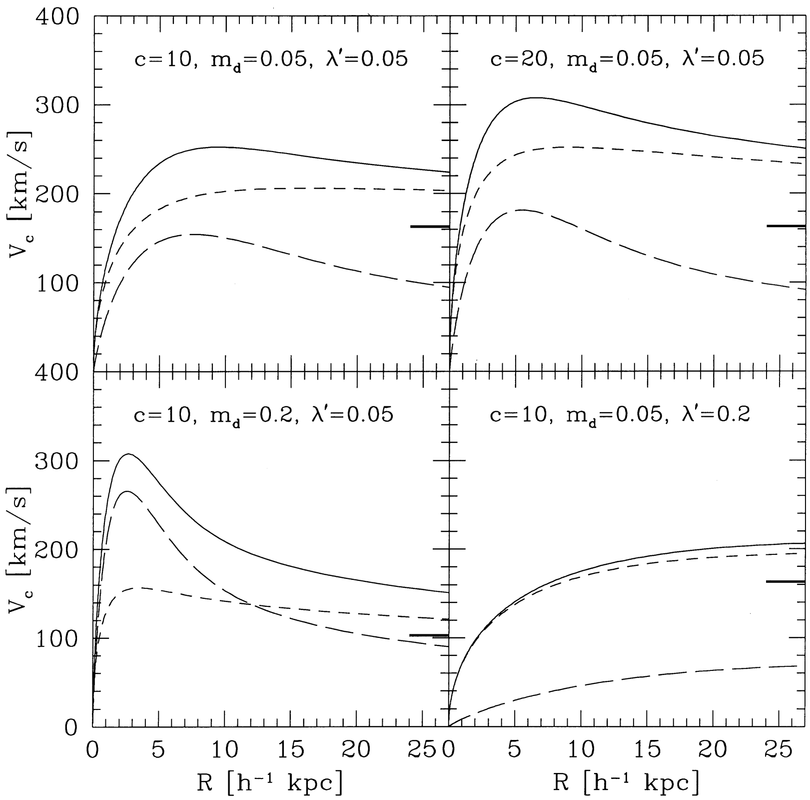

Figure 2. Rotation curves for disc galaxies formed in haloes with an initial density distribution described by the NFW profile. The shape of the rotation curves depends only on the concentration parameter, c, the fraction of mass in the disc, $m_{\rm d}$, and the spin parameter, $\lambda' \equiv (j_{\rm d}/m_{\rm d})\lambda$. The total mass of a halo determines both the disc scalelength and the amplitude of the rotation curve. Four panels are shown for different sets of c, $m_{\rm d}$ and λ'. The disc mass is assumed to be $M_{\rm d} = 5\times 10^{10} h^{-1}\,{\rm M}_\odot$. The rotation velocities induced by the disc and the dark matter are shown using long-dashed and short-dashed lines, respectively, while the total rotation velocity is shown by a solid line. The rotation velocity induced by the disc reaches a peak at about two disc scalelengths. The rotation velocity at r_{200} is indicated by thick horizontal bars and is identical to the rotation velocity at all radii for a singular isothermal sphere with the same mass. The upper left panel should be viewed as the reference panel. Only one parameter is varied between this panel and any other. Notice how both the prominence and amplitude of the peak in the rotation curve change between panels.

expression has sufficient accuracy:

$$f_R \approx \left(\frac{\lambda'}{0.1}\right)^{-0.06+2.71m_{\rm d}+0.0047/\lambda'}(1-3m_{\rm d}+5.2m_{\rm d}^2)$$
$$\times(1-0.019c+0.00025c^2+0.52/c), \tag{32}$$

where $\lambda' \equiv (j_{\rm d}/m_{\rm d})\lambda$. We will see in Section 3.1 that the rotation curves predicted by our procedure typically reach a maximum near $3R_{\rm d}$ and in much of the discussion which follows we will use the value at this point to characterize their amplitude. As a result, it is also useful to have a fitting formula for the dimensionless coefficient $f_V(\lambda, c, m_{\rm d}, j_{\rm d})$ in

$$V_{\rm c}(3R_{\rm d}) = \left(\frac{GM}{r_{200}}\right)^{1/2} f_V = V_{200} f_V. \tag{33}$$

We find

$$f_V \approx \left(\frac{\lambda'}{0.1}\right)^{-2.67m_{\rm d}-0.0038/\lambda'+0.2\lambda'}(1+4.35m_{\rm d}-3.76m_{\rm d}^2)$$
$$\times\frac{1+0.057c-0.00034c^2-1.54/c}{[-c/(1+c)+\ln(1+c)]^{1/2}}. \tag{34}$$

The approximations in (32) and (34) are accurate to within 15 per cent for $5 < c < 30$, $0.02 < \lambda' < 0.2$ and $0.02 < m_{\rm d} < 0.2$.

3 THE SYSTEMATIC PROPERTIES OF DISCS

3.1 Rotation curves

According to the model set out in Section 2.3 the shape of the rotation curve of a disc depends on the concentration of its halo, c, on the fraction of the halo mass which it contains, $m_{\rm d}$, and on its angular momentum as specified by the parameter combination $\lambda' = (j_{\rm d}/m_{\rm d})\lambda$. For given values of these three parameters the amplitude of the rotation curve and its radial scale are set by any single scale parameter, either for the halo (M, r_{200} or V_{200}) or for the disc ($M_{\rm d}$, $R_{\rm d}$ or Σ_0). Fig. 2 shows examples chosen to illustrate how changes in $m_{\rm d}$, λ' and c affect the shape of the rotation curve of a disc of fixed mass. Curves for other disc masses can be obtained simply by scaling both axes by $M_{\rm d}^{1/3}$. In all cases the rotation curves are flat at radii larger than a few disc scalelengths. At smaller radii the shape of the curves depends strongly on the spin parameter. For small values of λ' the disc is more compact, and its self-gravity is more important. The rotation velocity then increases rapidly near the centre to a peak near $R \sim 3R_{\rm d}$, thereafter dropping gradually towards a plateau at larger radii. For large λ', the disc is much more extended and its self-gravity is negligible. The rotation velocity then increases slowly with radius in the inner regions.

Since the surface density of a disc is roughly proportional to $(\lambda')^{-2}$, these results imply a correlation between disc surface

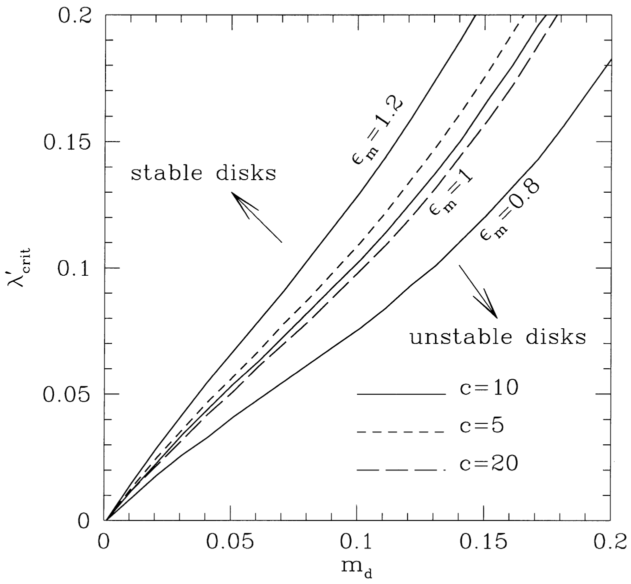

Figure 3. Critical values of λ' ($\equiv\lambda j_d/m_d$) for disc instability as a function of m_d. Results are shown for three choices of ϵ_m. For a given m_d, discs are stable if $\lambda' > \lambda'_{crit}$. The dependence on halo concentration, c, is weak, and is shown only for $\epsilon_m = 1$.

brightness and rotation curve shape which is very reminiscent of the observational trends pointed out by Casertano & van Gorkom (1991). Our predicted rotation curves also become more peaked at small radii for larger values of m_d, again because of the larger gravitational effect of the disc. Rotation curves as peaked as that shown in the lower left panel of Fig. 2 are not observed. As we will discuss below, this is probably because such discs are violently unstable. Halo concentration affects rotation curves in the obvious way; more strongly peaked curves are found in more concentrated haloes. Combining these trends we conclude that slowly increasing rotation curves are expected for low-mass discs in haloes with large λ' and small c. Since c is smaller for more massive haloes (see NFW), we would predict slowly rising rotation curves to occur preferentially in giant galaxies. In fact, the opposite is observed. This is almost certainly a result of the greater influence of the bulge in giant systems. A final trend which is clear from Fig. 2 is that at fixed disc mass, more strongly peaked curves have larger maximum rotation velocities. A similar trend can be seen in the observational data (e.g. Persic & Salucci 1991).

3.2 Disc instability

The modelling of the last two sections can lead to discs with a very wide range of properties. Not all of these discs, however, are guaranteed to be physically realizable. In particular, those in which the self-gravity of the disc is dominant are likely to be dynamically unstable to the formation of a bar. There is an extensive literature on such bar instabilities (see Christodoulou, Shlosman & Tohline 1995 and references therein). For our purposes the most relevant study is that of Efstathiou, Lake & Negroponte (1982) who used N-body techniques to investigate global instabilities of exponential discs embedded in a variety of haloes. They found the onset of the bar instability for stellar discs to be characterized by the criterion

$$\epsilon_m \equiv \frac{V_{max}}{(GM_d/R_d)^{1/2}} \lesssim 1.1, \tag{35}$$

where V_{max} is the maximum rotation velocity of the disc. The appropriate instability threshold for gas discs is lower, $\epsilon_m \lesssim 0.9$, as discussed in Christodoulou et al. (1995). In our model,

$$\epsilon_m \approx \frac{1}{2^{1/4}}\left(\frac{\lambda'}{m_d}\right)^{1/2} f_c^{-1/4} f_R^{1/2} f_V. \tag{36}$$

Thus, discs are stable if

$$\lambda' \gtrsim \lambda'_{crit} = \sqrt{2}\epsilon^2_{m,crit} m_d f_c^{1/2} f_R^{-1} f_V^{-2}, \tag{37}$$

where $\epsilon_{m,crit} \approx 1$ is the critical value of ϵ_m for disc stability. If the effect of disc self-gravity on R_d and V_c is weak, then $\lambda'_{crit} \sim m_d$. Fig. 3 shows λ'_{crit} as a function of m_d for our NFW models. Results are shown for $\epsilon_{m,crit} = 0.8$, 1, and 1.2, in order to bracket the critical values of ϵ_m discussed above. In practice we will normally adopt $\epsilon_{m,crit} = 1$ as a fiducial value. The dependence of λ'_{crit} on halo concentration is weak, because for a given m_d, the dependences of V_{max} and R_d on c are opposite. Since halo mass and assembly time affect λ'_{crit} only through c, we expect disc stability to be almost independent of these parameters. As one can see from Fig. 3, it is a useful rough approximation to take $\lambda' > m_d$ as the condition for stability. Thus in Fig. 2 the top two discs are marginally stable, the lower left disc is strongly unstable and the lower right disc is stable.

Disc galaxies are common and appear to be stable. If we take account of the expected distribution of λ (equation 15) and the likelihood that $j_d \leq m_d$, then the results in Fig. 3 suggest that m_d values of 0.05 or less will be needed to ensure that most haloes host stable discs rather than the descendants of unstable discs.

3.3 Disc scalelengths and formation times

For a given cosmogony our assumptions determine the joint distribution of disc size and rotation speed once values are adopted for the mass and angular momentum fractions, m_d and j_d, and for the disc formation redshift. This distribution can be compared directly with observation provided that our size measure, R_d, can be identified with the exponential scalelength of observed luminosity profiles. This seems reasonable since there is no evidence that the mass-to-light ratio of the stellar populations in real discs is a strong function of radius. In our simplified model the disc 'formation redshift' is just the time at which the arguments of Section 2 are applied. We make no attempt to follow the actual formation and evolution of discs, and we assume that all discs form at the same time. This formation redshift should be interpreted as the epoch when the material actually observed was assembled into a single virialized object.

Fig. 4 compares predicted distributions of R_d as a function of V_c with observational data for a large sample of nearby spirals. The four panels give predictions for formation redshifts of 0 and 1, and for two different cosmogonies, SCDM and ΛCDM; predictions for CCDM and τCDM are similar to those for SCDM. As a characteristic measure of rotation speed for our model galaxies we use the value of V_c at $3R_d$. As discussed in Section 2.3 this is always close to the maximum of the rotation curve. The solid line in each panel is the R_d–V_c relation for *critical* discs (i.e. those with $\lambda' = \lambda'_{crit}$) for the case $m_d = 0.05$; stable discs must lie above this line. Since $\lambda'_{crit} \approx 0.05$ in this case, and since, in general, we expect $j_d \leq m_d$, implying $\lambda' \leq \lambda$, at most half of all dark haloes will contain stable discs for $m_d \gtrsim 0.05$ (see the discussion around equation 15). The short-dashed line in each panel is the corresponding critical line for $m_d = 0.025$. In this case about 90 per cent of the dark haloes can host stable discs under the optimistic assumption that $j_d = m_d$. The critical lines would be even lower if $m_d < 0.025$, but values of λ

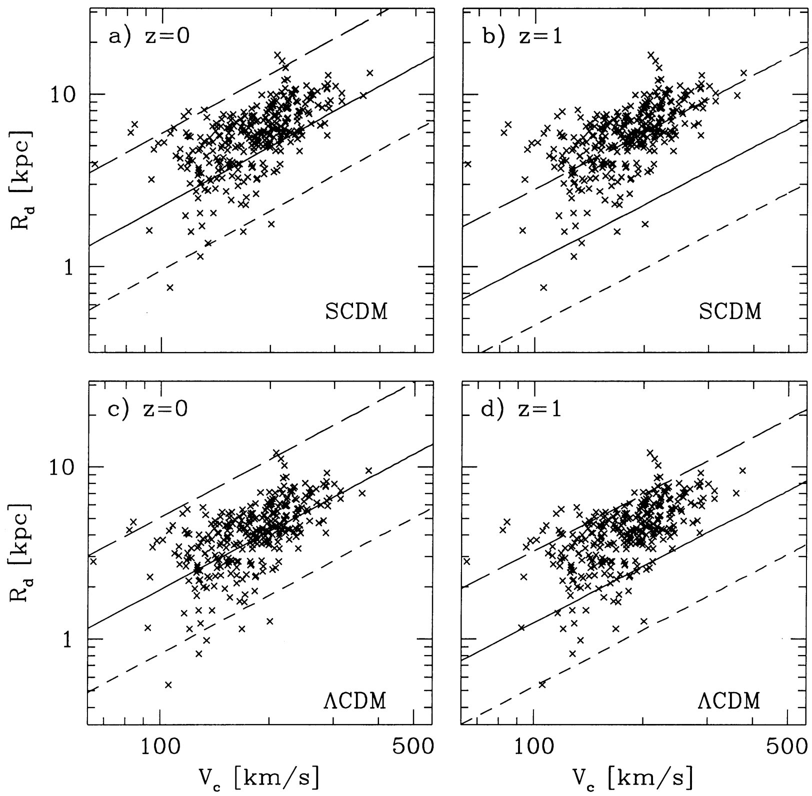

Figure 4. Model predictions for $R_{\rm d}$ as a function of $V_{\rm c}$ for stable discs assembled at $z=0$ and at $z=1$ in the SCDM and ΛCDM models. The solid lines give the relations for critical discs when $m_{\rm d}=0.05$, while short-dashed lines give the corresponding relations for $m_{\rm d}=0.025$. Stable discs must lie above the line for the relevant value of $m_{\rm d}$. The long-dashed lines correspond to $m_{\rm d}=j_{\rm d}$ and $\lambda=0.1$; at most 10 per cent of discs should lie above these lines. The data points are the observational results of Courteau (1996, 1997) for a sample of nearby normal spirals.

below 0.025 are rare, and so such compact discs will not be abundant unless $j_{\rm d}$ is often substantially smaller than $m_{\rm d}$. Finally, the long-dashed lines in Fig. 4 show $R_{\rm d}$–$V_{\rm c}$ relations for $m_{\rm d}=j_{\rm d}=0.05$ and $\lambda=0.1$. For these parameters disc self-gravity is negligible and the line is almost unaltered for $m_{\rm d}=j_{\rm d}=0.025$. Fewer than 10 per cent of the dark haloes have $\lambda \geq 0.1$ in the λ distribution of equation (15). Thus for $j_{\rm d} \leq m_{\rm d}$ very few discs are expected to lie above these long-dashed lines. The slopes and relative amplitudes of all the theoretical lines in Fig. 4 can easily be understood from the scalings in equation (12).

The data points in Fig. 4 are the observational results of Courteau and coworkers (Courteau 1996, 1997; Broeils & Courteau 1997) for *present-day* normal spirals. For a formation redshift of zero, the observed distribution lies comfortably below the long-dashed lines and above the short-dashed lines in both cosmologies. A significant fraction of the discs lie below the solid lines, particularly for ΛCDM, suggesting that these discs must have $m_{\rm d} \lesssim 0.05$ in order to be stable. For this formation redshift it seems relatively easy to reproduce the observed distribution in both cosmogonies. For a formation redshift of 1, in contrast, the observed points clearly lie too high relative to the predictions of the SCDM model (and similarly for CCDM and τCDM). Observed discs are too big to have formed at $z \sim 1$ in a high-density universe, unless there is some way for $j_{\rm d}$ to be substantially larger than $m_{\rm d}$. The observed points also lie rather high for $z=1$ in ΛCDM, but here the discrepancy is marginal provided that $j_{\rm d} \sim m_{\rm d}$ is indeed a realistic expectation. It is clear that substantial transfer of angular momentum from baryons to dark matter, resulting in $j_{\rm d} \ll m_{\rm d}$, would lead to unacceptably small discs for any assembly redshift in all of the cosmogonies we consider. This would also be the case if only the gas in central regions of the halo took part in the formation of the disc, because most of the angular momentum is initially possessed by the material in the outer parts of the halo (e.g. Warren et al. 1992; Eke, Navarro & Frenk 1997). Note that although the observed discs of Fig. 4 apparently formed late, this does not mean that discs were not present in large numbers at high redshift; early discs should, however, be significantly smaller than present-day objects of the same $V_{\rm c}$.

For the cosmogonies considered here, the comoving number density of galaxy-sized haloes is expected to peak at $z \sim 1$ and then to decline gradually at lower redshift. The peak density is comparable to the number density of galaxies observed today. Thus, as can be seen explicitly from more detailed semi-analytic modelling (e.g. Kauffmann et al. 1993), these models do indeed predict enough haloes to house the observed population of discs. Late formation thus appears viable in terms of both the structural properties and the abundance of discs in CDM-like models.

3.4 Disc surface densities

For a given cosmogony the distributions of M (the halo mass) and λ are known as a function of redshift (see equations A5 and 15), and furthermore the halo concentration factor, c, can be calculated from M and z (we neglect any scatter in c, see the Appendix). For any particular formation redshift, we can therefore generate Monte Carlo samples of the halo distribution in the M–λ plane, and, using specific values for $m_{\rm d}$ and $j_{\rm d}$, transform these into Monte Carlo samplings of the disc population. Fig. 5 shows the distribution

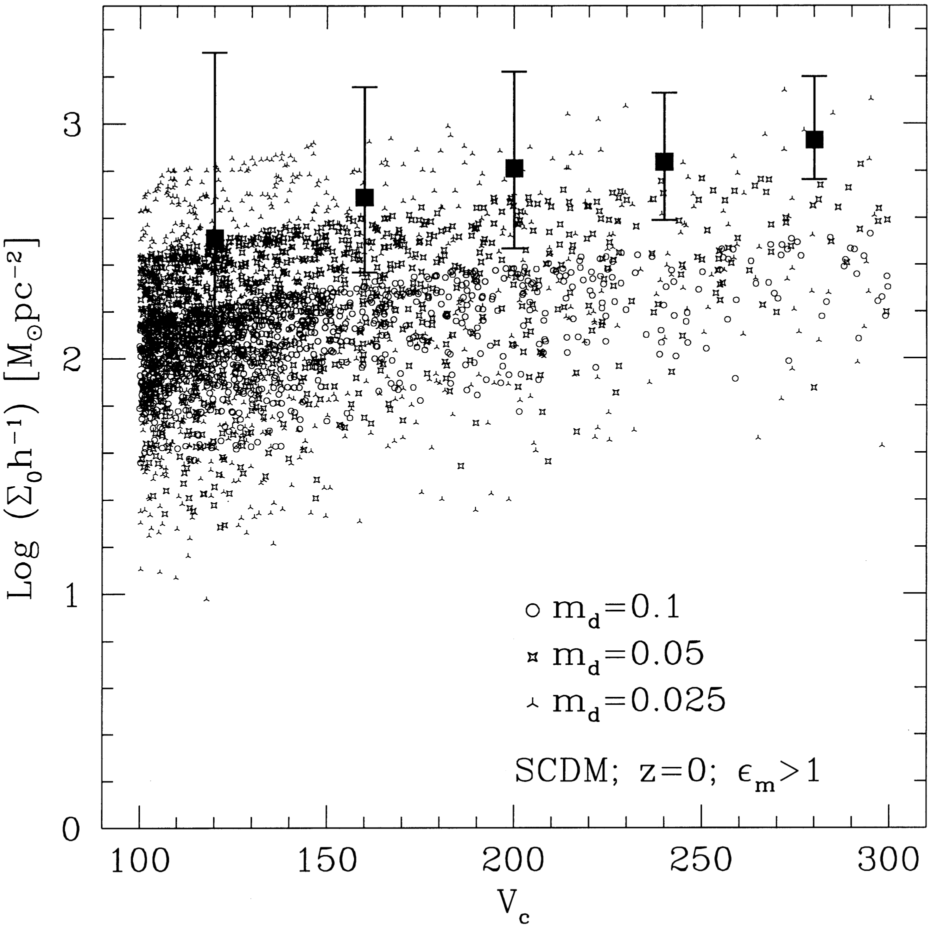

Figure 5. The distribution of central surface density for discs at $z = 0$ in the SCDM model. Results are shown assuming $m_d = j_d$ and for $m_d = 0.025$, 0.05 and 0.1. Only stable discs with $\epsilon_m > 1$ are plotted. The squares with error bars refer to the observational data from Fig. 4. The circular velocities have been converted to a luminosity using the Tully–Fisher relation of Giovanelli et al. (1997), and this in turn has been converted into a mass using $\Upsilon_I = 1.7h$ (Bottema 1997). The square is plotted at the median value in each bin and the ends of the error bars mark the upper and lower 10 per cent points of the distributions.

of discs in the V_c–Σ_0 plane for SCDM with $m_d = 0.025$, 0.5 and 0.1, $j_d = m_d$ and a formation redshift of zero. Unstable discs with $\epsilon_m < 1$ are excluded. The instability criterion leads to an upper cutoff in the central surface luminosity density Σ_0. For the simple isothermal sphere model of Section 2.2 this upper cutoff can be written as

$$\Sigma_{\rm crit} \propto \frac{m_d}{(\lambda'_{\rm crit})^2} H(z) V_c \propto \frac{V_c}{\lambda'_{\rm crit}} H(z) \propto \frac{V_c}{m_d} H(z), \qquad (38)$$

where we have used $\lambda'_{\rm crit} \approx m_d$ (see equation 37). Thus $\Sigma_{\rm crit}$ is larger for higher z, for higher V_c and for lower m_d. The last two dependences are clearly seen in Fig. 5.

To compare the distributions of Fig. 5 with real data we need to assume a stellar mass-to-light ratio for the discs. Throughout this article we will use the values found for high surface brightness discs by Bottema (1997). From disc dynamics, he inferred $\Upsilon_B = (1.79 \pm 0.48)$ for $h = 0.75$. Since $B - I = 1.7$ for a typical disc galaxy (McGaugh & de Blok 1997), and $(B - I)_\odot = 1.33$, we obtain $\Upsilon_I = (1.7 \pm 0.5)h$. Solid squares in Fig. 5 correspond to median values for the Courteau data in Fig. 4. We have converted from V_c to L_I using the Tully–Fisher relation of Giovanelli et al. (1997; equation 39), and from L_I to Σ_0 using equation (6) and $\Upsilon_I = 1.7\,h$. Error bars join the upper and lower 10 per cent points of the distribution in each V_c bin. The typical central surface brightnesses found in this way are similar to the 'standard' value advocated by Freeman (1970). For $m_d = 0.05$, the median central surface density for discs at $z = 0$ in SCDM appears to be about a factor of 2 too faint compared with the observed value. However, this discrepancy should not be over-interpreted since low surface brightness galaxies are probably under-represented in Courteau's sample. In addition, the model prediction has substantial uncertainties. For a given V_c, the predicted disc surface density is proportional to $H(z)$, and so a formation redshift of 0.5 would increase the predictions by a factor of 1.8. Furthermore, the upper cutoff of the disc surface density distribution depends sensitively on the value of $\epsilon_{\rm m,crit}$ (cf. equation 35). For a given m_d, $\Sigma_{\rm crit} \propto \epsilon_{\rm m,crit}^{-4}$; a 20 per cent decrease in $\epsilon_{\rm m,crit}$ would thus increase the upper cutoff on Σ_0 by a factor of two.

Despite these uncertainties, Fig. 5 suggests that $m_d \lesssim 0.05$ is preferred. Notice that this conclusion is independent of the R_d–V_c analysis of the last section which suggested similar values for m_d. It is interesting that the abundance of both high and low surface density galaxies is predicted to increase as m_d decreases. This is a consequence of the wider range of λ values which produce stable discs when m_d is small. There is currently considerable debate about the relative abundance of low surface brightness (LSB) galaxies. Our results confirm those of Dalcanton et al. (1997); hierarchical models can relatively easily produce a spread which appears broad enough to be consistent with the observations. We note that an

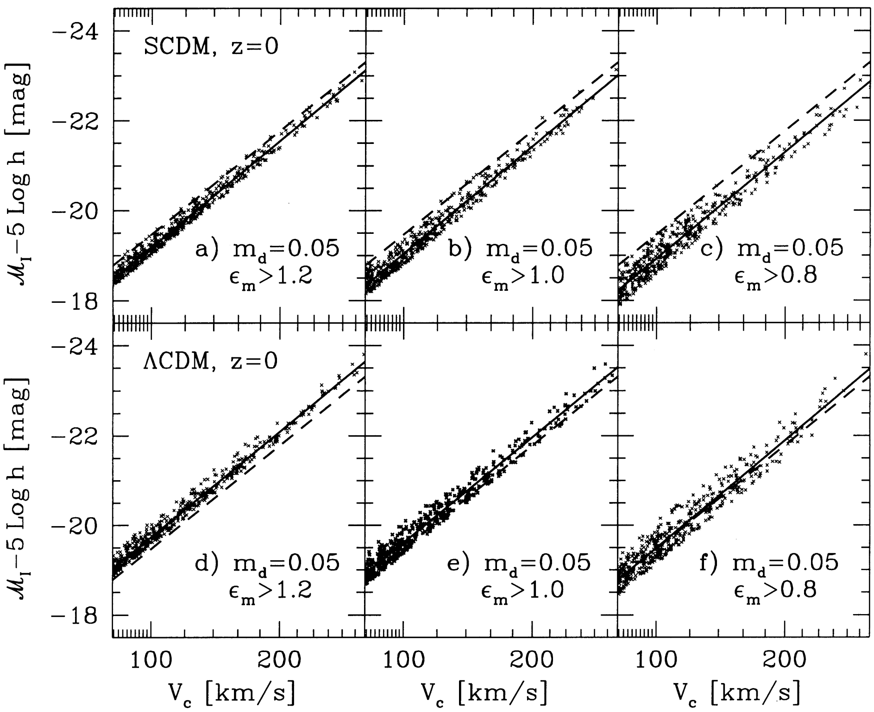

Figure 6. Tully–Fisher (TF) relations for stable discs at $z = 0$ in the SCDM and ΛCDM cosmogonies. Monte Carlo samples of the predicted luminosity–rotation velocity distribution are shown for three choices of ϵ_m. We have converted stellar mass (in the model) into *I*-band luminosity using $\Upsilon = 1.7h$ (Bottema 1997). The solid lines give the linear regressions of absolute magnitude against log V_c. The dashed lines show the observed TF relation as given by Giovanelli et al. (1997).

additional uncertainty in any detailed comparison comes from the fact that the star formation efficiency in discs may well vary strongly as a function of surface density. This would further complicate the conversion between disc mass and disc light.

3.5 Tully–Fisher relations

In one of the most complete recent studies of the Tully–Fisher relation for nearby galaxies, Giovanelli et al. (1997) put together a homogeneous set of H I velocity profiles and *I*-band photometry for a set of 555 spiral galaxies in 24 clusters. By careful adjustment of the relative zero-points of the different clusters they derived a TF relation in the (Cousins) *I* band,

$$\mathcal{M}_I - 5\log h = -(21.00 \pm 0.02) - (7.68 \pm 0.13)(\log W - 2.5), \tag{39}$$

where W is the inclination-corrected width of the H I line profile, and, to a good approximation, is twice the maximum rotation velocity. When comparing with our models we will assume $W = 2V_c(3R_d)$ (see Section 2.3). Giovanelli et al. find a mean scatter around this relation of 0.35 mag, but point out that the scatter is actually magnitude dependent; it increases significantly with decreasing velocity width. A nearly identical Tully–Fisher relation was derived independently by Shanks (1997), but the zero-point of the TF relation in Willick et al. (1996) is fainter by about 0.2 mag.

In order to derive luminosities for the discs in our models we need to specify their stellar mass-to-light ratio. Unfortunately, the appropriate value for this quantity is quite uncertain; here we will again use the value $\Upsilon_I = 1.7h$ which Bottema (1997) derived for the discs of high surface brightness spirals. For a given mass-to-light ratio, the magnitude of a disc galaxy can be calculated as

$$\mathcal{M}_I = \mathcal{M}_{\odot,I} - 2.5\log\frac{\mathrm{L}_I}{\mathrm{L}_{\odot,I}}$$
$$= 4.15 - 2.5\log\frac{M_\mathrm{d}}{\mathrm{M}_\odot} + 2.5\log(\Upsilon_I), \tag{40}$$

where we have used $\mathcal{M}_{\odot,V} = 4.83$, and $(V - I)_\odot = 0.68$ (Bessel 1979, table II). Note that in the observed TF relation $\mathcal{M}_I$ is the total absolute magnitude of the galaxy, whereas for our models we are estimating the absolute magnitude of the disc alone; we are therefore implicitly assuming that the bulge luminosity can be neglected for the galaxies under consideration (but see Section 5 below).

With these assumptions, we can generate a Monte Carlo disc catalogue, as in Section 3.4, and plot $\mathcal{M}_I$ versus $V_c(3R_d)$ ($\approx W/2$). Fig. 6 shows such plots for stable discs with a formation redshift of $z = 0$ in SCDM and ΛCDM. Here we assume $m_d = j_d = 0.05$. For each cosmogony, the three panels show results for three choices of $\epsilon_{m,crit}$, the critical value of ϵ_m for disc instability (equations 35 to 37). As one can see, the plots are similar in all cases. The zero-point for the SCDM model is lower than that for the ΛCDM model, for the reasons to be discussed in more detail in Section 3.5.3. The scatter is slightly larger for smaller values of $\epsilon_{m,crit}$, because discs are then stable for smaller λ values where disc self-gravity is more important. By fitting plots such as these we can clearly derive TF relations for our models, and so can compare their slope, scatter and zero-point with those of the observed Tully–Fisher relation.

3.5.1 Tully–Fisher slopes

We begin by considering the slopes of the model relations. The solid lines in Fig. 6 are the linear regressions of $\mathcal{M}_I$ on V_c for each Monte Carlo sample of simulated data. It is clear that in all cases the slope

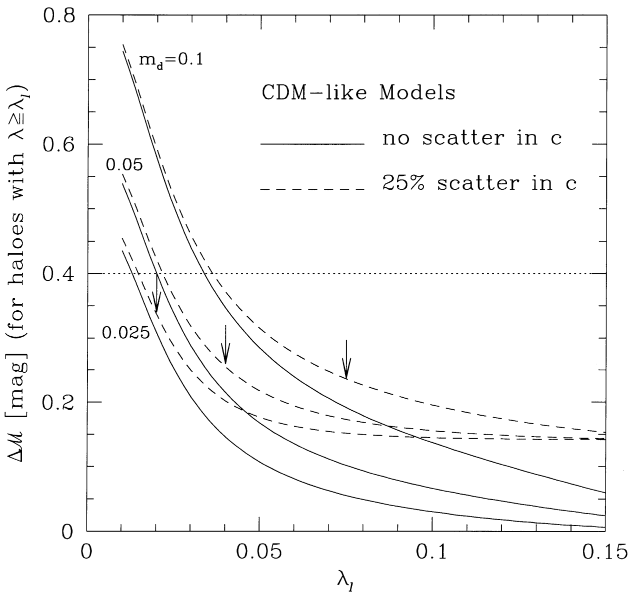

Figure 7. The scatter about the mean TF relation as a function of λ_l, the lower limit on λ for the haloes included in the relation. The solid curves show results which ignore the scatter caused by variations of the halo concentration, c, while the dashed curves show an rms scatter of 25 per cent in c. Three curves are shown for three different disc mass fractions, $m_d = 0.1, 0.05$ and 0.025 (from top to bottom). The horizontal line shows the observed scatter for normal disc galaxies, as given by Willick et al. (1996). The arrows mark the critical values of λ; discs are stable only for larger λ values.

is close to $\alpha = 3$ (where α is defined in equation 16), and is consistent with the observed value of Giovanelli et al. which we indicate with a dashed line. Although there is clearly very good agreement, it is important to realize that this is a consequence of choosing to compare with the observed *I*-band data. In fact, the observed slope is quite dependent on the photometric band used. For example, in the *B*-band it is about $\alpha = 2.5$ (Strauss & Willick 1995 and references therein). This difference arises because the colours of disc galaxies vary systematically with their luminosity; fainter galaxies show proportionately more star formation and are bluer. Stellar population models suggest that the stellar mass-to-light ratios of discs must vary quite strongly with luminosity in the *B* band (being smaller for the fainter, bluer galaxies) but could plausibly be constant at *I*. For this reason the *I*-band TF relation does indeed appear to be the most appropriate one to compare with our models.

In the models the slight deviation of the slope from $\alpha = 3$ is caused by the fact that massive haloes are less concentrated than low-mass haloes. To see this, we recall NFW's discovery that the concentration factor of a halo is determined by its formation time z_f; massive haloes form later and so are less concentrated (see the Appendix). Since the value of f in equation (A10) is small, we have $\delta_{z_f} - \delta_c \propto \sigma(fM)$. For galactic haloes, $\sigma(fM) \gg 1$ in all the cosmogonies considered here, and so $\delta_{z_f} - \delta_c \approx \delta_{z_f} \propto (1 + z_f)$. Writing the rms mass fluctuation defined in equation (A4) as $\sigma^2(r_0) \propto r_0^{-(3+n_{\rm eff})}$, we have $(1 + z_f) \propto (fM)^{-(3+n_{\rm eff})/6}$. On galactic scales, the effective power index $n_{\rm eff} \sim -2$ for our CDM models, so that more massive haloes have lower values of z_f, and so also of c. The value of α is slightly larger for SCDM, because $n_{\rm eff}$ is slightly larger in this case. As shown by Navarro et al. (1997), if $n_{\rm eff}$ differs substantially from -2, then α can be very different from 3. The effect of changing the *amplitude* of the fluctuation spectrum is negligible, and the slope is also insensitive to changes in m_d, j_d, and the formation redshift of discs, provided that none of these parameters varies with V_c. The observed slope of the TF relation is thus a generic prediction of hierarchical models with CDM-like fluctuation spectra.

3.5.2 Tully–Fisher scatter

The observed scatter in the TF relation is quite small; Giovanelli et al. (1997) quote 0.35 mag as an overall measure of scatter, while Willick et al. (1995, 1996) find 0.4 mag to be typical. It is clear from Fig. 6 that we do indeed predict a small scatter, but it is important to understand why. In the model of Section 2.2 the gravitational effect of discs is neglected, all haloes of the same mass have identical singular isothermal density profiles, and all discs have the same m_d and Υ_d. With these assumptions the TF relation has no scatter even though the broad λ-distribution leads to a wide range of disc sizes and surface brightnesses. In the more realistic model of Section 2.3, scatter in the TF relation can arise from two effects. For given disc and halo masses, the maximum rotation is larger for more compact discs, i.e. for those residing in more slowly spinning haloes. As a result, the scatter in the λ-distribution of haloes translates into a scatter about the predicted TF relation. This is the source of scatter in Fig. 6; this scatter remains small because the stability requirement eliminates the most compact systems. In addition, even for given M_d, M and λ, the disc rotation velocity will be larger in more concentrated haloes. Thus any scatter in c will produce scatter in the TF relation. We now examine the consequences of these two effects in detail.

The solid curves in Fig. 7 show the scatter about the mean model TF relations as a function of λ_l, an assumed lower limit on λ for the haloes allowed to contribute observable discs. For given m_d, this function is sensitive neither to cosmological parameters nor to the redshift of disc formation. The scatter increases as haloes with lower values of λ are included, because disc self-gravity becomes important for such systems. It increases with m_d, because the contribution of a disc to the rotation velocity is then larger at fixed λ. It is clear that the predicted scatter can be made sufficiently small, provided that discs with large m_d and small λ are excluded. The arrows next to each curve in Fig. 7 show the smallest value of λ for which discs with the given value of m_d are stable (here we conservatively require $\epsilon_m > 0.8$). It is clear that the predicted scatter is smaller than observed if $m_d \gtrsim 0.025$. For even smaller m_d, a larger range of λ is allowed for stable discs, leading to a larger scatter. This is a consequence of the deviation between the NFW profile and an isothermal sphere. Since only about 10 per cent of haloes have $\lambda < 0.025$, the increased scatter in this case is due to a relatively small number of compact outliers.

The distribution of the halo concentration factor at fixed mass is poorly known. In the simulations of NFW, the rms scatter in c is $\Delta c/c \approx 25$ per cent. To demonstrate the effect of such scatter on the predicted TF relation, the dashed curves in Fig. 7 show the predicted scatter if we assume a 25 per cent rms uncertainty in the concentration parameter of haloes of a given mass. (Note: NFW show that the scatter in c is uncorrelated with λ.) If this variability in halo profiles is indeed realistic, it is clear from Fig. 7 that it adds relatively little scatter to the TF relation. As NFW point out, this is in conflict with the conclusions of Eisenstein & Loeb (1996) from an analytic assessment of the expected variation in halo profiles. In summary, the analysis of this section suggests that it may not be difficult for hierarchical models to produce a disc population with Tully–Fisher scatter within the observed limits. We note, however, that we have

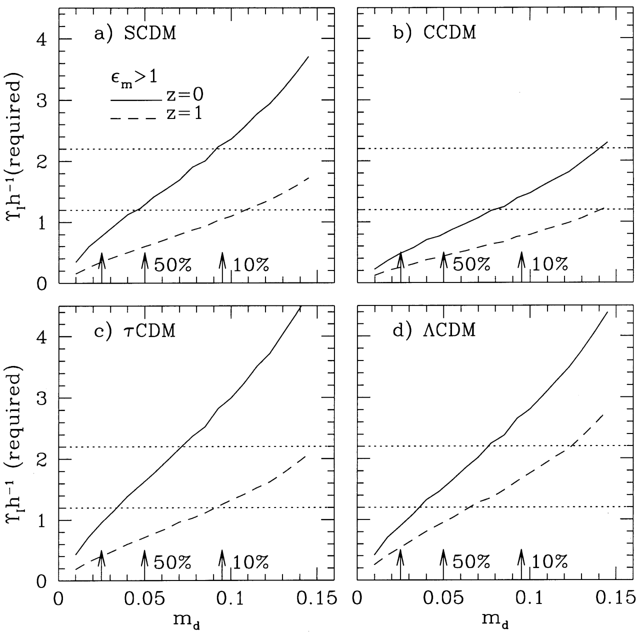

Figure 8. The mass-to-light ratio required to reproduce the observed zero-point of the TF relation as given by Giovanelli et al. (1997). Stable discs with $\epsilon_m > 1$ are used. Results are shown for two assembly redshifts, $z = 0$ (solid lines) and $z = 1$ (dashed lines). The horizontal lines bracket the values of Υ_I allowed by dynamical studies of discs (Bottema 1997). The arrows indicate the values of m_d at which 90, 50 and 10 per cent of haloes can host stable discs.

not included the bulge contribution to the luminosity of the galaxies or possible variations in Υ_d. Both presumably act to increase the TF scatter. Furthermore, the small scatter predicted may also hinge upon the assumption that present-day discs formed over a narrow range of redshifts. Although this assumption is consistent with our inference from disc sizes, any scatter in the formation time would, nevertheless, also act to increase the TF scatter.

3.5.3 The Tully–Fisher zero-point

The zero-point of the predicted TF relation depends weakly on the distribution of λ and on our stability requirement. On the other hand, it depends strongly on m_d, the fraction of the halo mass in discs, on Υ_d, the stellar mass-to-light ratio of the discs, and on z, the redshift at which disc material is assembled within a single dark halo. Fig. 8 shows the values of $\Upsilon_d h^{-1}$ required to reproduce the observed zero-point of the I-band TF relation (equation 39) as a function of m_d. Zero-points are calculated for stable discs with $\epsilon_m > 1$ (the results are very similar for $\epsilon_m > 0.8$ or > 1.2). In all cases the required mass-to-light ratio is approximately proportional to m_d. The three arrows in each panel show the values of m_d at which 10, 50 and 90 per cent of the haloes can host stable discs.

Stable disc galaxies are common and there are no obvious observational counterparts for a large number of 'failed' unstable discs. The $z = 0$ lines in this figure thus suggest $\Upsilon_d < 1h$ in the I band for the CCDM model, whereas for SCDM, ΛCDM and τCDM the upper limit gets progressively weaker. This trend is a consequence of the steadily decreasing concentration of haloes of given mass along this sequence, which results in a corresponding decrease in the maximum rotation velocity. The same trend can be seen quite clearly in Fig. 6. The maximum allowed mass-to-light ratio is even smaller for higher assembly redshifts, because discs are then less massive for a given V_c. The horizontal dotted lines in Fig. 8 bracket the $\pm 1\sigma$ range derived by Bottema (1997) from his analysis of the dynamics of observed discs. This range takes account of the fact that some (dim) discs may have as much as half of their mass in gas. As one can see, in order to reproduce the Tully–Fisher zero-point with Υ_I in the allowed range, normal discs could form at high z only if m_d is large, while for low formation redshifts $m_d < 0.05$ is possible. For $m_d > 0.05$ most haloes *cannot* host stable discs, so we infer that normal spiral discs must form late with an effective assembly redshift close to zero. A reasonable zero-point then requires $m_d \gtrsim 0.03$, in good agreement with the values obtained above from the observed sizes and surface brightnesses of discs. Finally we note that because disc self-gravity is less important for larger values of λ, somewhat higher mass-to-light ratios are needed if LSB galaxies are to fit on the same Tully–Fisher relation as normal spirals.

4 HIGH-REDSHIFT DISCS AND DAMPED Lyα SYSTEMS

Damped Lyα absorption systems (DLS), corresponding to absorbing clouds with a neutral column density, $N_{\rm H\,I} \gtrsim 2\times10^{20}\,{\rm cm}^{-2}$, are seen in the spectra of many high-redshift QSOs. Their abundance varies very roughly as $n(z) \sim 0.03(1+z)^{1.5}$ over the redshift range $1.5 < z < 4$, and their total H I content is a few tenths of a per cent of the critical density, about the same as the total mass in stars in the local Universe (see e.g. Storrie-Lombardi et al. 1996). Over the last decade Wolfe and his collaborators have used a wide range of observational indicators, most recently the velocity structure in the associated metal lines, to argue that these systems correspond to large equilibrium discs with $V_c \gtrsim 200\,{\rm km\,s^{-1}}$, the extended and gas-rich progenitors of present-day spirals (Wolfe et al. 1986; Lanzetta, Wolfe & Turnshek 1995; Wolfe 1995; Prochaska & Wolfe 1997, but see Jedamzik & Prochaska 1997). Early theoretical studies showed that the total H I content of these systems can be reproduced in some but not all hierarchical cosmologies, provided that systems with circular velocities well below 200 ${\rm km\,s^{-1}}$ are allowed to contribute (Mo & Miralda-Escudé 1994; Kauffmann & Charlot 1994; Ma & Bertschinger 1994; Klypin et al. 1995). A detailed study of the standard CDM cosmology by Kauffmann (1996b) concluded that discs in all haloes down to $V_c \sim 50\,{\rm km\,s^{-1}}$ must contribute, once a realistic model for star formation is included. Numerical simulations by Gardner et al. (1997) led these authors to a similar conclusion, while higher resolution simulations by Haehnelt, Steinmetz & Rauch (1997) showed that the kinematic data of Prochaska & Wolfe (1997) can be reproduced by non-equilibrium discs in low-mass haloes and so do not *require* large V_c. None of these simulations included star formation. Cross-sections derived from them should, perhaps, be viewed with caution since even in the best case the numerical resolution is similar to the disc scalelengths we predict. Furthermore, the underlying physical assumptions lead to a substantial underprediction of the sizes of present-day discs. On the other hand, these simulations suggest that most of the absorption cross-section at high redshift is contributed by merging systems which are far from equilibrium, particularly in a high-density universe. If this is true then our model of centrifugally supported discs may not be appropriate.

Our models allow a more detailed study of the sizes and cross-sections of high-redshift discs than does that of Kauffmann (1996b). Fig. 9 shows how the predicted abundance of absorbers at $z = 2.5$ rises as discs within lower and lower mass haloes are allowed to

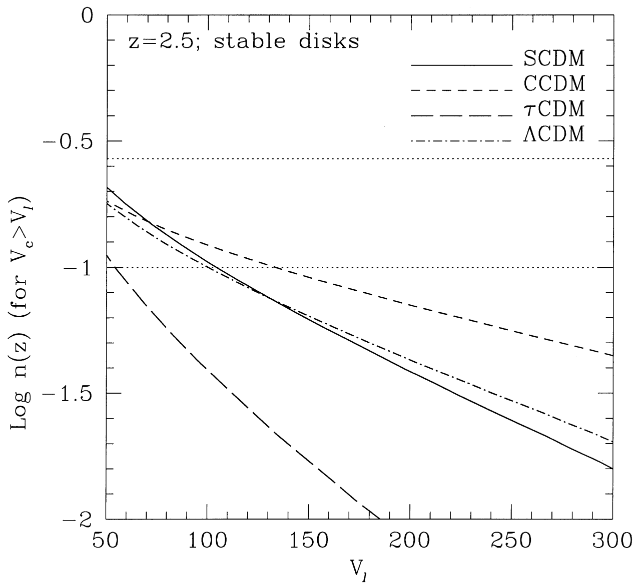

Figure 9. Logarithm of the predicted abundance of damped Lyα systems at $z = 2.5$ as a function of V_l, the rotation velocity of the least massive discs allowed to contribute. Only stable discs are assumed to give rise to damped Lyα systems (i.e. discs with $\epsilon_\mathrm{m} > 1$). The horizontal lines show the $\pm 2\sigma$ range of the observed abundance as given by Storrie-Lombardi et al. (1996).

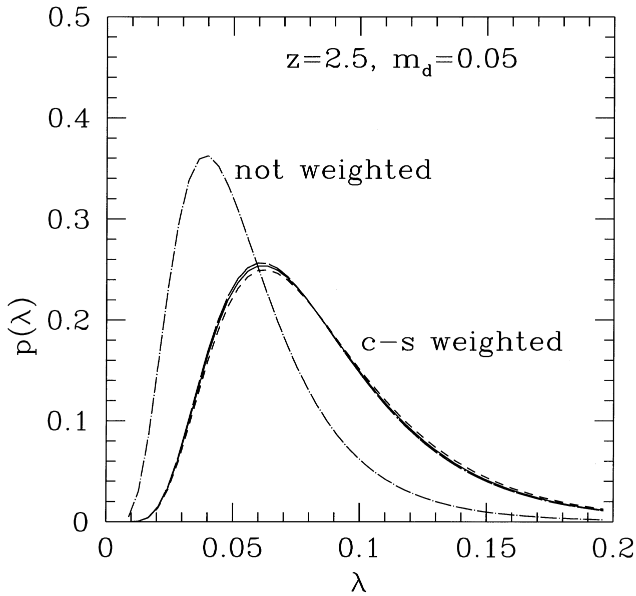

Figure 10. The cross-section (c-s) weighted distribution of halo spin at $z = 2.5$. Notice that this distribution depends only weakly on cosmogony; the curves corresponding to our four cosmogonies can barely be distinguished. The unweighted λ-distribution, as given by equation (15), is shown as the dot-dashed curve.

contribute. We parametrize the mass of the smallest contributing halo by V_l, the rotation velocity of its central disc measured at $3R_\mathrm{d}$ and averaged over the λ-distribution of stable discs. This abundance refers to absorbers with $N_{\mathrm{H\,I}} > N_\mathrm{l}$ and is calculated from

$$n(z) = \frac{\pi}{2}(1+z)^3 \frac{\mathrm{d}l}{\mathrm{d}z} \int \mathrm{d}\lambda p(\lambda) \int_{N_\mathrm{l}}^{\infty} \frac{\mathrm{d}N_{\mathrm{H\,I}}}{N_{\mathrm{H\,I}}^3} \int_{M_\mathrm{l}}^{\infty} \mathrm{d}M \times n_h(M,z) R_\mathrm{d}^2(M,\lambda,z) N_0^2(M,\lambda,z) \times (1+2x_\mathrm{l})\mathrm{e}^{-2x_\mathrm{l}} \Theta(\epsilon_\mathrm{m} - \epsilon_\mathrm{m,crit}), \quad (41)$$

where $l(z)$ is the proper distance at redshift z, $n_h(M,z)\mathrm{d}M$ is the comoving number density of galactic haloes given by equation (A5), N_0 is the central column density of the disc, $N_\mathrm{l} = 2\times 10^{20}\,\mathrm{cm}^{-2}$ is the minimum H I column density for a DLS, and $x_\mathrm{l} = -\ln[\min(1, N_{\mathrm{H\,I}}/N_0)]$. The step function, $\Theta(x) = 1$ for $x > 0$ and $\Theta(x) = 0$ for $x \le 0$, ensures that only stable discs are used. For this plot we assume $m_\mathrm{d} = j_\mathrm{d} = 0.05$ and $\epsilon_\mathrm{m,crit} = 1$. We also assume that all baryons at the outer edge of the absorbing region are in the form of H I gas, and that the column density never drops below N_l at smaller radii. This may be unrealistic at low redshift because star formation may substantially reduce the mass of H I gas. The horizontal dotted lines show a $\pm 2\sigma$ range for the observed DLS abundance at $z = 2.5$, taken from Storrie-Lombardi et al. (1996). The lower limit on V_l needed to reproduce the observations can be read off immediately. This limit varies quite strongly between cosmogonies. For τCDM, which has the smallest power on galactic scales, one has to include discs with rotation velocities smaller than $50\,\mathrm{km\,s^{-1}}$. This confirms the result found earlier for the MDM model which has a similar power spectrum (Mo & Miralda-Escudé 1994; Kauffmann & Charlot 1994; Ma & Bertschinger 1994; Klypin et al. 1995). For the other three models, about one-third of the observed systems can arise in discs with $V_\mathrm{c} \gtrsim 200\,\mathrm{km\,s^{-1}}$, and two-thirds or more in discs with $V_\mathrm{c} \gtrsim 100\,\mathrm{km\,s^{-1}}$. It may not be difficult to accommodate discs with V_c as large as suggested by Wolfe and collaborators, although these will be predicted to be much smaller at $z = 2.5$ than nearby discs with the same circular velocity.

It is interesting that the total cross-section of rotationally supported *stable* discs with $V_\mathrm{c} \gtrsim 100\,\mathrm{km\,s^{-1}}$ can already explain the observations. Unless the formation of such discs is prevented, they should give rise to a large fraction of the observed DLS. Some absorbers may correspond to *unstable* discs, but the abundance of this population should be relatively small; such discs are compact and so have small cross-sections. Fig. 10 shows the cross-section weighted distribution of the spin parameter for discs at $z = 2.5$. Comparing this with the unweighted λ distribution (shown as the dot-dashed curve), we see that absorption comes primarily from discs with large λ. For $m_\mathrm{d} = j_\mathrm{d} = 0.05$, $\lambda_\mathrm{crit} \approx 0.05$, and less than 20 per cent of DLS are produced by unstable systems (assuming, of course, that instability does not change the cross-section). The value of $n(z)$ for stable discs is maximized for $m_\mathrm{d} \sim 0.05$, but varies little for m_d ($= j_\mathrm{d}$) in the range from 0.025 to 0.07. The abundance is smaller both for larger and for smaller m_d, in the first case because the number of stable discs is small, and in the second because the amount of gas is small. This range is similar to the one we inferred in earlier sections from the properties of local disc galaxies. As shown by Haehnelt et al. (1997), many DLS may be produced by gas that has not fully settled into centrifugal equilibrium. We are implicitly assuming that the cross-section for damped absorption does not vary strongly, at least on average, over this settling period.

It is also instructive to look at the predicted distribution of the impact parameter b, defined as the distance between the line of sight and the centre of a disc that produces a DLS. This distribution can be written as

$$P(b)\mathrm{d}b \propto \mathrm{d}b \int \mathrm{d}\lambda p(\lambda) \int_{M_\mathrm{l}}^{\infty} \mathrm{d}M n_h(M,z) \Theta(\epsilon_\mathrm{m} - 1) \times F[N_0(M,\lambda,z)/N_\mathrm{l}, b, R_\mathrm{d}(M,\lambda,z)], \quad (42)$$

where M_l is the lower limit on halo mass, and F is the distribution of

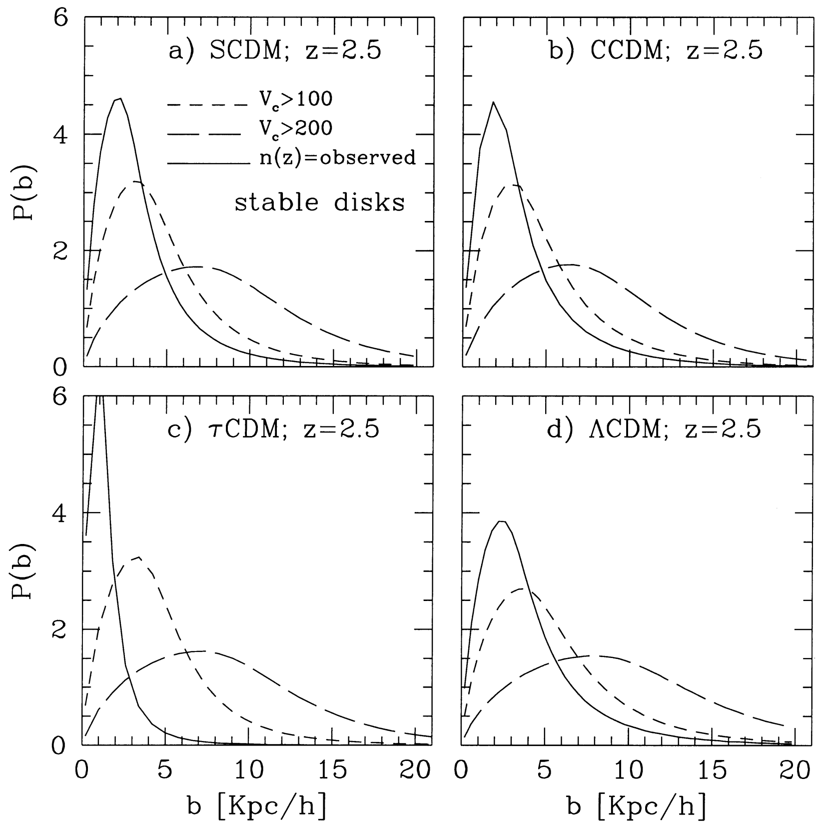

Figure 11. The distribution of impact parameter for damped systems in stable discs at $z = 2.5$. The solid curves show the results when the mass of the smallest contributing discs is chosen so that the predicted abundance of absorbers is equal to the observed value. The dashed curves show the results when only discs with large V_c are selected.

b for a disc with scalelength R_d and central surface density N_0 observed at a random inclination angle. The function F can be obtained from simple Monte Carlo simulations. The solid curves in Fig. 11 show $P(b)$ at $z = 2.5$, with M_l chosen to reproduce the observed abundance of DLS. For τCDM, this distribution is narrow and peaks at quite small values of b; DLS at large impact parameters are rare in this model. For the other three models, however, the upper quartile of the distribution is at $\sim 5\,h^{-1}$ kpc, so systems with relatively large impact parameter do occur. Not surprisingly, they tend to be associated with high-V_c discs, as can be seen from the dashed curves. At present, there are very few measurements of the impact parameter for a high-redshift DLS. Djorgovski et al. (1996) have identified a galaxy responsible for a DLS at $z = 3.15$, and for this case the impact parameter is about $13\,h^{-1}$ kpc (for $q_0 = 0.1$). An observation by Lu, Sargent & Barlow (1997) suggests that this is indeed a rotating disc, with $V_c \sim 200\,\mathrm{km\,s^{-1}}$. As one can see from Fig. 11, for this V_c, the observed impact parameter is not exceptionally large. One cannot draw any statistical conclusions from a single event, but if systems like this turn out to be common the τCDM model would be disfavoured.

It is worth noting that this consistency with the observational results requires that m_d be in the range 0.025 to 0.07, and that little angular momentum be transferred to the dark halo during disc formation. Significant angular momentum loss would produce smaller discs. Haloes with smaller V_c would then have to be included in order to match the observed abundance. In this case, typical DLS would be predicted to have smaller V_c and smaller b, but to have larger column densities. Substantial star formation would be required to reduce the column densities to the observed values, contradicting, perhaps, the low metal abundances measured in high-redshift DLS.

The galaxies responsible for DLS are likely to be easier to identify at lower redshift. It is therefore interesting to make predictions for such systems. As an example, we show the impact parameter distribution for DLS at $z = 1$ in Fig. 12. Results are shown only for SCDM and ΛCDM; those for CCDM and τCDM are similar. The redshift is chosen to be typical for the low-redshift DLS observed by, for example, Steidel et al. (see Steidel 1995). In computing this distribution we have used only discs with $V_c = 100$–$300\,\mathrm{km\,s^{-1}}$. This choice is based on the fact that discs with smaller V_c are difficult to identify, while those with larger V_c are rare. An upper limit on V_c has to be imposed in our calculation, because massive haloes are likely to host elliptical galaxies or galaxy clusters which contain only a small amount of H I gas. The median and the upper quartile of the distribution are at about 7 and $10\,h^{-1}$ kpc, respectively (see the solid curves). Larger impact parameters are expected for samples biased towards galaxies with larger V_c (see the dashed curves). As before, of course, these predictions assume that star formation has not substantially reduced the gas column near the damped absorption boundary. Some decrease in impact parameter may therefore be expected by $z = 1$. However, the absorption cross-section of an exponential disc depends only logarithmically on m_d, and so Fig. 12 will not change much provided that star formation is only moderately efficient in the outer galaxy. On the other hand, the H I mass in a DLS decreases in proportion to m_d, so that systems observed at lower redshift may have systematically lower column densities and so give rise to a smaller cosmic density parameter in H I. These

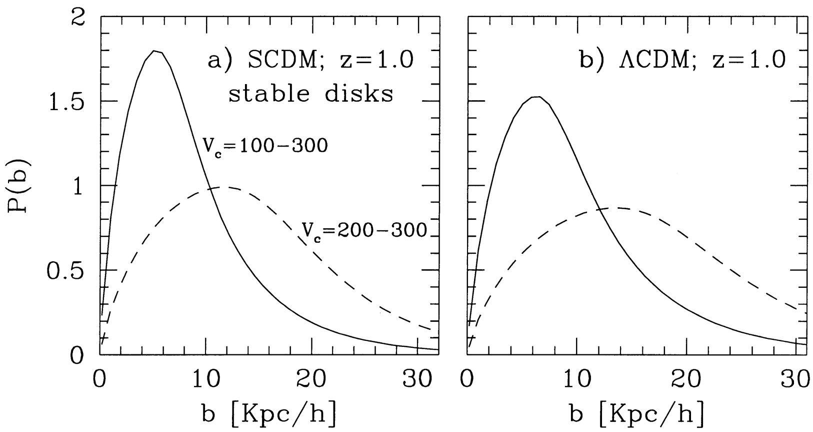

Figure 12. The distribution of impact parameter for damped systems in stable discs at $z = 1$. Results are shown for two ranges of V_c.

trends are indeed observed (Wolfe 1995), and arise naturally in models that take star formation into account (Kauffmann & Charlot 1994; Kauffmann 1996b).

To see what kind of discs produce DLS at low redshifts, we can examine the cross-section weighted distribution of the spin parameter. This distribution depends only weakly on z, so that Fig. 10 is still relevant. Notice again the strong bias towards the large λ tail. As discussed in Section 3, the discs that form in haloes with large λ have large size and low surface densities. We thus expect that galaxies selected as DLS will be biased towards low surface densities. As noted by McGaugh & de Blok (1997) and others, the star formation rates in such galaxies are low, giving rise to low surface brightnesses, and producing a relatively small reduction in their cross-section for damped absorption. The impact parameter distribution of Fig. 12 may then apply. There are now some observations of galaxies responsible for low-redshift DLS. Steidel et al. (see Steidel 1995) find the typical impact parameter for such systems to be 5–15 h^{-1} kpc. There are also indications that these galaxies tend to be blue, with low surface brightness (Steidel 1995) and low chemical abundance (Pettini et al. 1995). All these points seem to agree well with our expectations. Obviously, more such data will provide stringent constraints on disc formation models of the kind we propose here.

5 THE EFFECT OF A CENTRAL BULGE

So far we have considered galaxies to contain only disc and halo components. In reality, most spirals also contain a bulge. For a galaxy of Milky Way type or later, the bulge mass is less than 20 per cent that of the disc, so its dynamical effects are small. For earlier type spirals, however, the bulge makes up a larger fraction of the stellar mass, and its effects may be significant. In this section we use a simple model to assess how our results are affected by the presence of a central bulge. We assume bulges to be point-like, to have a mass which is m_b times that of the halo, and to have negligible angular momentum. Further, we assume either that the specific angular momentum of the disc is the same as that of its dark halo (so that $j_d = m_d$ as usually assumed above), or that the total specific angular momentum of the stellar components is equal to that of the halo (so that $j_d = m_d + m_b$). The second case may be appropriate if angular momentum transfer to the halo is negligible, if low angular momentum gas forms the bulge, and if high angular momentum gas settles into the disc.

Under these assumptions it is straightforward to extend the model of Section 2.2 to include the bulge. Equation (25) becomes

$$M_f(r) = M_d(r) + M(r_i)(1 - m_d - m_b) + M_b, \qquad (43)$$

and $V^2_{c,DM}$ in equations (30) and (31) is replaced by $V^2_{c,DM}(r) + V^2_{c,b}(r)$, where $V^2_{c,b}(r) = GM_b/r$ is the contribution to the circular velocity from the bulge. With these changes, the procedure of Section 2.2 can be applied as before to obtain the disc scalelength, R_d, and the rotation curve, $V_c(R)$.

In Fig. 13 we show the predicted rotation curves when disc and bulge masses are equal. Results are shown for the two cases mentioned above, namely $j_d = m_d$ and $j_d = m_d + m_b = 2m_d$. The same total halo mass and concentration are adopted as in the top left panel of Fig. 2. The rotation curves now diverge at small radius because of our unrealistic assumption of a point-like bulge. In the case where $j_d = 2m_d$ the disc is substantially more extended, and the value of V_c at given radius is slightly lower, than in the case where $j_d = m_d$.

To see the effect of the central bulge more clearly, we compare values of R_d and $V_c(3R_d)$ for the two cases, $M_b = M_d$ and $M_b = 0$. Fig. 14 shows how the relative values vary with $m_d + m_b$. This figure assumes $\lambda = 0.05$ and $c = 10$, but in fact the ratios are quite insensitive to λ and c. As one can see, for $j_d = m_d$ the values of R_d and V_c do not change much even when half of the accreted gas is put into the central bulge. On the other hand, for $j_d = 2m_d$, the disc scalelength increases by a factor of 2, and the rotation velocity drops significantly below that for $M_b = 0$. This case produces similar results to those for $\lambda = 0.1$ and $M_b = 0$.

The results in Fig. 14 have some interesting implications. If discs have the same specific angular momentum as their dark haloes, and if the luminosity of a galaxy is proportional to its total stellar mass, then the zero-point of the TF relation is almost independent of the mass of the bulge. Even in the extreme case where $M_d = M_b$ and discs have twice the specific angular momentum of their haloes, the disc rotation velocity for given $M_d + M_b$ is only reduced by about 20 per cent provided $m_d + m_b \lesssim 0.1$. If disc and bulge had the same mass-to-light ratio, this would change the zero-point of the TF relation by about -0.8 mag, but since the stellar mass-to-light ratio of bulges is undoubtedly higher than that of discs, the actual change would be smaller. In practice, most of the galaxies used in applications of the TF relation have bulge-to-disc ratios much smaller than one, so we expect the effects of the bulges to produce little scatter in the TF relation.

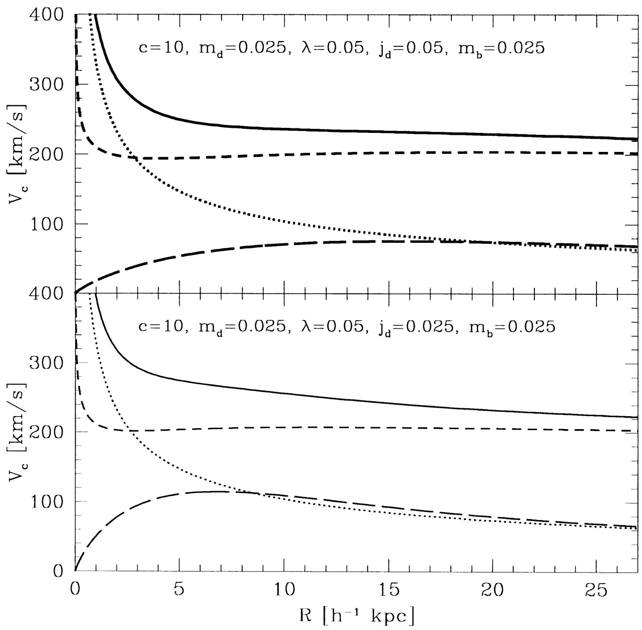

Figure 13. Rotation curves for disc galaxies with central bulges (cf. Fig. 2). The disc and the bulge are assumed to have the same mass, $2.5\times10^{10}\,h^{-1}\,\mathrm{M}_{\odot}$. The circular velocities induced by the disc, the bulge and the dark matter are shown by long-dashed, dotted and short-dashed lines, respectively. The total circular velocity is shown by the solid line. In the top panel, the disc is assumed to have twice as much specific angular momentum as the dark matter, while in the bottom panel the two specific angular momenta are assumed to be the same. The central cusps in these rotation curves reflect our unrealistic assumption of a point-mass bulge.

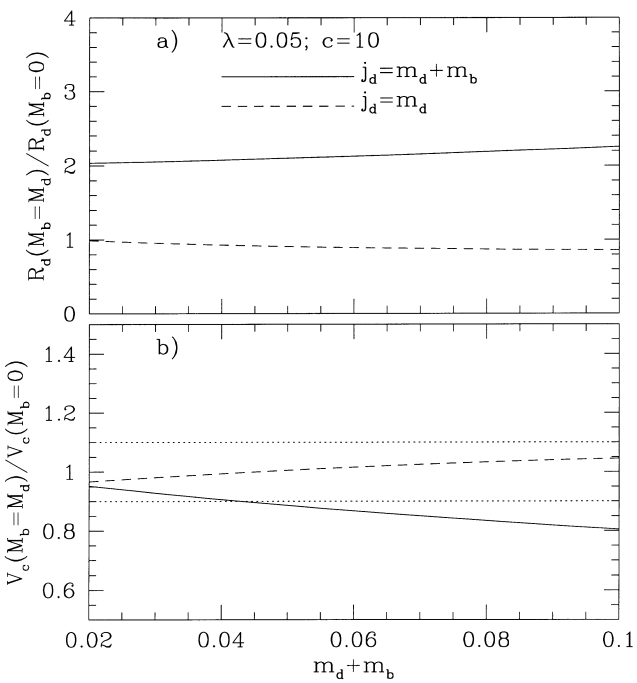

Figure 14. Disc scalelength, $R_{\rm d}$, and disc rotation velocity, $V_{\rm c}(3R_{\rm d})$, in a model where the mass of the central bulge ($M_{\rm b}$) is equal to that of the disc ($M_{\rm d}$), as functions of the total stellar mass fraction, $m_{\rm d}+m_{\rm b}$. Results are shown in units of the values when $M_{\rm b}$ is set to zero. We have assumed $\lambda=0.05$ and $c=10$. The solid curves show the results for $j_{\rm d}=m_{\rm d}+m_{\rm b}$, while the dashed curves show those for $j_{\rm d}=m_{\rm d}$. The two dotted lines give a rough indication of the scatter in the observed TF relation.

6 DISCUSSION

In this paper, we have formulated a simple model for the formation of disc galaxies. Although many of the observed properties of spirals and damped Lyα absorbers seem relatively easy to explain, it is important to keep in mind our underlying assumptions. These leave open a number of difficult physical questions. We have assumed that all galaxy haloes have the universal density profile proposed by NFW. This appears relatively safe since the original NFW claims have been confirmed by a number of independent N-body simulations (e.g. Tormen, Bouchet & White 1996; Cole & Lacey 1996; Huss, Jain & Steinmetz 1997). More significantly we assume that all discs have masses and angular momenta which are fixed fractions of those of their haloes. Successful models require $M_{\rm d}/M \lesssim 0.05$ and $J_{\rm d}/J \approx M_{\rm d}/M$. These relations are not produced in a natural way by existing simulations of hierarchical galaxy formation. While it is common to find all the gas associated with galactic haloes within condensed central objects (so that $M_{\rm d}\propto M$), the gas usually loses most of its angular momentum to the dark matter during galaxy assembly. This results in $J_{\rm d}/J \ll M_{\rm d}/M$ and produces discs which are too small (Navarro & Benz 1991; Navarro & White 1994; Navarro & Steinmetz 1997). The resolution of this problem may be related to the well-known need to introduce strong feedback in order to get a viable hierarchical model for galaxy formation (e.g. White & Rees 1978; White & Frenk 1991; Kauffmann et al. 1993). Such feedback is not included in the simulations, but is required in hierarchical models to suppress early star formation in small objects, thus ensuring that gas remains at late times to form large galaxies and the observed intergalactic medium. Discs may then form from gas which remains diffuse and so loses little angular momentum during protogalactic collapse (e.g. Navarro et al. 1995). Unfortunately, while such effects may solve the angular momentum problem, they call into question the proportionality between disc mass and halo mass. The disc/halo mass ratios required by our models are, in any case, much less than the observed baryon mass fractions in rich galaxy clusters, so substantial inefficiency in assembling the galaxies is necessary in any consistent model.

Recently Dubinski, Mihos & Hernquist (1996) have suggested that the long tidal tails observed in some interacting galaxies may limit the mass of dark haloes. Their argument is simple. For given disc structure, more massive haloes lead to faster encounters and to deeper potential wells. Thus the perturbation on each of the discs is weaker, and the tails must contend with stronger restoring forces. Dubinski et al. studied N-body simulations of four different galaxy models, and found long tidal tails only in those with halo masses less than 10 times that of the disc(+bulge). Our models suggest haloes substantially more massive than this, but there may be no contradiction. In a prograde parabolic encounter between similar disc galaxies, the relative increase in specific kinetic energy of disc stars is approximately $\Delta E/V_{\rm c}^2 \propto V_{\rm c}^2/V_{\rm e}^2(R_{\rm p})$, where $V_{\rm e}(R_{\rm p})$ is the escape velocity at $R_{\rm p}$ and the constant of proportionality depends on the orbit geometry and the radius of the star's orbit relative to the minimum separation, $R_{\rm p}$ (see e.g. Binney & Tremaine 1987, Section 7). Furthermore, the depth of the confining potential may be compared with the energy with which a tail is launched using the ratio $\mathcal{E}\equiv[V_{\rm e}(R)/V_{\rm c}]^2$, where R is the initial radius of the tail material. Thus for close encounters where $R_{\rm p}$ and R differ by a relatively small factor, we can take $\mathcal{E}(2R_{\rm d})$ as the parameter characterizing the difficulty of making long tails; we choose $R=2R_{\rm d}$ here because about half of the disc material lies outside this radius. The value of $\mathcal{E}$ is about 5.7 for our fiducial model with $m_{\rm d}=0.05$, $\lambda=0.05$ and $c=10$, and it varies from 4.0 to 6.5 over the range of parameters we consider reasonable. For the four models studied by Dubinski et al. (1996), in order of increasing halo mass, we estimate $\mathcal{E} = 4.2, 5.5, 7.2$ and 9.3. The first two of these models made long tidal tails while the last two did not. We conclude that our fiducial model should make tails about as easily as their model B, and that none of our allowed models should be incapable of making tails despite the fact that their haloes are much more than 10 times as massive as their discs. The apparent difference in conclusions arises because haloes in our model are more centrally concentrated than in the simulations of Dubinski et al, thus decreasing $\mathcal{E}$. As we saw in Section 2.2, our models predict the mass and structure of haloes of given disc mass to depend only weakly on cosmology. We therefore expect tail-making ability to give at best weak constraints on cosmological parameters.

There are other interesting theoretical issues that are not addressed in this paper. As is well known, disc galaxies, especially LSB galaxies, have lower correlation amplitudes than ellipticals (see e.g. Davis & Geller 1976; Mo et al. 1992; Jing, Mo & Börner 1991; Mo, McGaugh & Bothun 1994). Since hierarchical clustering predicts little correlation between the spin parameter of a halo and its large-scale environment, this observed clustering difference cannot be considered a consequence of disc galaxies being associated with haloes with large λ. However, as discussed above, disc galaxies, especially LSBs, form late in our model. On the other hand, elliptical galaxies, and in particular cluster ellipticals, form at relatively high redshifts in hierarchical models (Kauffmann 1996a). Since, for given mass, haloes at low redshift are less correlated than those at high redshift (Mo & White 1996), the morphology dependence of clustering can arise as a consequence of the morphology dependence of formation time. This effect is seen quite clearly in the detailed semi-analytic galaxy formation models of Kauffmann et al. (1993) and Kauffmann, Nusser & Steinmetz (1997). Local environmental effects may also lead to morphological segregation: for example, extended discs may be destroyed in a high-density environment by tidal effects and gas stripping (Moore et al. 1996). Detailed modelling is clearly needed for any quantitative comparison with observation.

In this paper we have considered the formation of disc galaxies only. It is interesting to examine how other populations might fit into such a scenario. Earlier semi-analytic modelling has shown that many of the global properties of giant ellipticals can be understood if they formed by mergers between disc systems which themselves formed at early times in overdense 'protocluster' regions. As we have seen, high-redshift discs should be substantially denser and more compact than present-day discs of similar mass. This may go a long way towards explaining the high densities of observed ellipticals. Some bulges and ellipticals may also form in dark haloes with low spin where any disc would be too dense to be stable. Such 'spheroidal' systems may have systematically different properties from those that formed by mergers. We intend to return to a number of these issues in future papers.

ACKNOWLEDGMENTS

We are grateful to S. Courteau for providing the data plotted in Fig. 4. We thank Luiz da Costa for helpful discussions. This project is partly supported by the 'Sonderforschungsbereich 375-95 für Astro-Teilchenphysik' der Deutschen Forschungsgemeinschaft.

REFERENCES

Bardeen J., Bond J. R., Kaiser N., Szalay A. S., 1986, ApJ, 304, 15
Barnes J., White S. D. M., 1984, MNRAS, 211, 753
Baugh C. M., Cole S., Frenk C. S., Lacey C. G., 1997, preprint (astro-ph/9703111)
Bertschinger E., 1985, ApJS, 58, 39
Bessel M. S., 1979, PASP, 91, 589
Binney J., Tremaine S., 1987, Galactic Dynamics. Princeton Univ. Press, Princeton, NJ
Blumenthal G. R., Faber S. M., Flores R., Primack J. R., 1986, ApJ, 301, 27
Bottema R., 1997, A&A, 328, 517
Broeils A. H., Courteau S., 1997, in Persic M., Salucci P., eds, ASP Conf. Ser. 117, Dark and Visible Matter in Galaxies. Astron. Soc. Pac., San Francisco, p. 39
Carroll S. M., Press W. H., Turner E. L., 1992, ARA&A, 30, 499
Casertano S., Van Gorkom J., 1991, AJ, 101, 1231
Catelan P., Theuns T., 1996, MNRAS, 282, 436
Christodoulou D. M., Shlosman I., Tohline J. E., 1995, ApJ, 443, 551
Cole S., Lacey C., 1996, MNRAS, 281, 1176
Cole S., Aragon-Salamanca A., Frenk C. S., Navarro J. F., Zepf S. E., 1994, MNRAS, 271, 781
Courteau S., 1996, ApJS, 103, 363
Courteau S., 1997, AJ, 114, 2402
Dalcanton J. J., Spergel D. N., Summers F. J., 1997, ApJ, 482, 659 (DSS)
Davis M., Geller M., 1976, ApJ, 208, 13
Djorgovski S. G., Pahre M. A., Bechtold J., Elston R., 1996, Nat, 382, 234
Dubinski J., Mihos J. C., Hernquist L., 1996, ApJ, 462, 576
Efstathiou G., Lake G., Negroponte J., 1982, MNRAS, 199, 1069
Efstathiou G., Bond J. R., White S. D. M., 1992, MNRAS, 258, 1P
Eisenstein D. J., Loeb A., 1996, ApJ, 459, 432
Eke V. R., Navarro J. F., Frenk C. S., 1997, preprint (astro-ph/9708070)
Fall S. M., Efstathiou G., 1980, MNRAS, 193, 189
Freeman K., 1970, ApJ, 160, 811
Gardner J. P., Katz N., Weinberg D. H., Hernquist L., 1997, ApJ, 486, 42
Giovanelli R., Haynes M. P., da Costa L. N., Freudling W., Salzer J. J., Wegner G., 1997, ApJ, 477, L1
Gunn J., Gott R., 1972, ApJ, 176, 1
Haehnelt M. G., Steinmetz M., Rauch M., 1997, preprint (astro-ph/9706201)
Huss A., Jain B., Steinmetz M., 1997, preprint (astro-ph/9703014)
Jedamzik K., Prochaska J. X., 1997, preprint (astro-ph/9706290)
Jing Y. P., Mo H. J., Börner G., 1991, A&A, 252, 449
Kauffmann G., 1996a, MNRAS, 281, 487
Kauffmann G., 1996b, MNRAS, 281, 475
Kauffmann G., Charlot S., 1994, ApJ, 430, L97
Kauffmann G., White S. D. M., Guiderdoni B., 1993, MNRAS, 264, 201
Kauffmann G., Nusser A., Steinmetz M., 1997, MNRAS, 286, 795
Klypin A., Borgani S., Holtzman J., Primack J., 1995, ApJ, 444, 1
Lacey C., Cole S., 1993, MNRAS, 262, 627
Lacey C., Cole S., 1994, MNRAS, 271, 676
Lanzetta K. M., Wolfe A. M., Turnshek D. A., 1995, ApJ, 440, L435
Lu L., Sargent W. L. W., Barlow T. A., 1997, AJ, 115, 55
Ma C. P., Bertschinger E., 1994, ApJ, 434, L5
McGaugh S. S., de Blok W. J. G., 1997, ApJ, 481, 689
Mo H. J., Miralda-Escudé J., 1994, ApJ, 430, L25
Mo H. J., White S. D. M., 1996, MNRAS, 282, 347
Mo H. J., Einasto M., Xia X. Y., Deng Z. G., 1992, MNRAS, 255, 382
Mo H. J., McGaugh S. S., Bothun G. D., 1994, MNRAS, 267, 129
Mo H. J., Jing Y. P., White S. D. M., 1996, MNRAS, 282, 1096
Moore B., Katz N., Lake G., Dressler A., Oemler A., Jr, 1996, Nat, 379, 613
Navarro J. F., Benz W., 1991, ApJ, 380, 320
Navarro J. F., Steinmetz M., 1997, ApJ, 478, 13
Navarro J. F., White S. D. M., 1994, MNRAS, 267, 401
Navarro J. F., Frenk C. S., White S. D. M., 1995, MNRAS, 275, 56
Navarro J. F., Frenk C. S., White S. D. M., 1996, ApJ, 462, 563
Navarro J. F., Frenk C. S., White S. D. M., 1997, ApJ, 487, 73 (NFW)
Persic M., Salucci P., 1991, ApJ, 285, 307
Pettini M., King D. L., Smith L. J., Hunstead R. W., 1995 in Meylan G. ed., QSO Absorption Lines. Springer, Berlin p. 71
Press W. H., Schechter P., 1974, ApJ, 187, 425 (PS)
Prochaska J. X., Wolfe A. M., 1997, ApJ, in press

Shanks T., 1997, MNRAS, 290, L77
Steidel C. C., 1995, in Meylan G. ed., QSO Absorption Lines. Springer, Berlin p. 137
Steinmetz M., Bartelmann M., 1995, MNRAS, 272, 570
Storrie-Lambardi L. J., McMahon R. G., Irwin M. J., 1996, MNRAS, 283, L79
Strauss M., Willick J. A., 1995, Phys. Rep., 261, 271
Tormen G., Bouchet F. R., White S. D. M., 1997, MNRAS, 286, 865
Turner M. S., 1996, preprint (astro-ph/9610158)
Walker T. P., Steigman G., Schramm D. N., Olive K. A., Kang H.-S., 1991, ApJ, 376, 51
Warren M. S., Quinn P. J., Salmon J. K., Zurek W. H., 1992, ApJ, 399, 405
White S. D. M., Frenk C. S., 1991, ApJ, 379, 52
White S. D. M., Rees M. J., 1978, MNRAS, 183, 341
White M., Scott D., 1996, Comments Astrophys., 8, No. 5
White S. D. M., Efstathiou G., Frenk C., 1993, MNRAS, 262, 1023
Willick J. A., Courteau S., Faber S. M., Burstein D., Dekel A., 1995, ApJ, 446, 12
Willick J. A., Courteau S., Faber S. M., Burstein D., Dekel A., Kolatt T., 1996, ApJ, 457, 460
Wolfe A., 1995, in Meylan G. ed., QSO Absorption Lines. Springer, Berlin, p. 13
Wolfe A., Turnshek D. A., Smith H. E., Cohen R. D., 1986, ApJS, 61, 249

APPENDIX A: COSMOGONIES

We assume that the universe is dominated by cold dark matter (CDM). The initial power spectrum is

$$P(k) \propto kT^2(k), \tag{A1}$$

with

$$T(k) = \frac{\ln(1+2.34q)}{2.34q} \times \left[1 + 3.89q + (16.1q)^2 + (5.46q)^3 + (6.71q)^4\right]^{-1/4} \tag{A2}$$

and

$$q \equiv \frac{k}{\Gamma h\,\mathrm{Mpc}^{-1}} \tag{A3}$$

(see Bardeen et al. 1986). Following Efstathiou et al. (1992), we have introduced a shape parameter, Γ, for the power spectrum. The rms mass fluctuation in top-hat windows with radius r_0, $\sigma(r_0)$, is defined by

$$\sigma^2(r_0) = \frac{1}{2\pi^2}\int_0^\infty \frac{\mathrm{d}k}{k} k^3 P(k) W^2(kr_0), \tag{A4}$$

where $W(x)$ is the Fourier transform of the top-hat window function. The power spectrum, $P(k)$, is normalized by specifying $\sigma_8 \equiv \sigma(8\,h^{-1}\mathrm{Mpc})$.

We use the Press–Schechter formalism (Press & Schechter 1974) to calculate the mass function of dark haloes. In this formalism, the comoving number density of dark haloes, with mass in the range $M \rightarrow M + \mathrm{d}M$, at redshift z is

$$n_h(M,z)\mathrm{d}M = -\left(\frac{2}{\pi}\right)^{1/2} \frac{\overline{\rho}_0}{M}\frac{\delta_z}{\sigma(r_0)}\frac{\mathrm{d}\ln\sigma(r_0)}{\mathrm{d}\ln M} \times \exp\left[-\frac{\delta_z^2}{2\sigma^2(r_0)}\right]\frac{\mathrm{d}M}{M}, \tag{A5}$$

where $\overline{\rho}_0$ is the mean matter density of the universe at present time; M is the mass of the halo, related to the initial comoving radius r_0 of the region from which the halo formed (measured in current units) by $M = \frac{4\pi}{3}\overline{\rho}_0 r_0^3$; and δ_z is the threshold linear overdensity for collapse at redshift z. According to the spherical collapse model,

$$\delta_z = (1+z)\delta_c \frac{g(a_0)}{g(a)}, \tag{A6}$$

where $\delta_c \approx 1.68$ (see NFW); $g(a)$ is the linear growth factor at the expansion factor a corresponding to the redshift z (a_0, the present value of a, is taken to be 1):

$$g(a) = \frac{5}{2}\Omega\left[\Omega^{4/7} - \Omega_\Lambda + (1+\Omega/2)(1+\Omega_\Lambda/70)\right]^{-1} \tag{A7}$$

(see Carroll, Press & Turner 1992), with

$$\Omega \equiv \Omega(a) = \frac{\Omega_0}{a + \Omega_0(1-a) + \Omega_{\Lambda,0}(a^3 - a)}, \tag{A8}$$

$$\Omega_\Lambda \equiv \Omega_\Lambda(a) = \frac{a^3\Omega_{\Lambda,0}}{a + \Omega_0(1-a) + \Omega_{\Lambda,0}(a^3 - a)}. \tag{A9}$$

To put the NFW density profile in a cosmological context, we need to calculate the concentration factor c defined in equation (20). For this density profile, c is related to the characteristic overdensity, δ_0, by equation (21). The appropriate value of c depends on halo formation history and on cosmology. NFW proposed a simple model for c based on halo formation time. The formation redshift z_f of a halo identified at $z = 0$ with mass M is defined as the redshift by which half of its mass is in progenitors with mass exceeding fM, where $f < 1$ is a constant. According to the formula given by Lacey & Cole (1993) based on the Press–Schechter formalism, the halo formation time is then defined implicitly by

$$\mathrm{erfc}\left\{\frac{(\delta_{z_f} - \delta_c)}{\sqrt{2[\sigma^2(fM) - \sigma^2(M)]}}\right\} = \frac{1}{2}. \tag{A10}$$

NFW found that the characteristic overdensity of a halo at $z = 0$ is related to its formation redshift z_f by

$$\delta_0(M,f) = C(f)\Omega_0\left[1 + z_f(M,f)\right]^3, \tag{A11}$$

where the normalization $C(f)$ depends on f. We will take $f = 0.01$ as suggested by the N-body results of NFW. In this case $C(f) \approx 3\times 10^3$. Thus, for a halo of given mass at $z = 0$, one can obtain the concentration factor c from equations (A6)–(A11). In practice, we first solve z_f from equation (A10) and insert the value of z_f into equation (A11) to get δ_0; we then use this value of δ_0 in equation (21) to solve for c. The distribution of c is not well known. In the simulations of NFW, the scatter in c is $\Delta c/c \approx 0.25$.

Equations (A10)–(A11) can be easily extended to calculate concentrations for haloes identified at $z > 0$. In this case, we just replace δ_c in equation (A10) by δ_z, and Ω_0 in equation (A11) by $\Omega(a)/(1+z)^3$, where a is the scalefactor at z.

This paper has been typeset from a TEX/LATEX file prepared by the author.